DAS Departamento de Automação e Sistemas
CTC Centro Tecnológico
UFSC Universidade Federal de Santa Catarina

Scanner-based wire fed laser cladding process: a case study

Relatório submetido à Universidade Federal de Santa Catarina
como requisito para a aprovação na disciplina
DAS 5511: Projeto de Fim de Curso

Denise Albertazzi Gonçalves

Florianópolis, setembro de 2016

Scanner-based wire fed laser cladding process: a case study

Denise Albertazzi Gonçalves

Esta monografia foi julgada no contexto da disciplina
DAS5511: Projeto de Fim de Curso
e aprovada na sua forma final pelo
Curso de Engenharia de Controle e Automação

Prof. *Walter Lindolfo Weingaertner*

_____
Assinatura do Orientador

Banca Examinadora:

Dr. Stefan Kaierle
Orientador na Empresa

Prof. Dr. Walter Lindolfo Weingaertner
Orientador no Curso

Alexander Barroi
Orientador na Empresa

Prof. Dr. João Carlos Espíndola Ferreira
Avaliador

Felippe Schmoeller da Roza
Hugo Gutierrez Sigolo
Debatedores

Acknowledgements

To Prof. Dr. Walter Lindolfo Weingaertner and Prof. Dr. Stefan Kaierle for the given opportunity and financial aid.

To Eng. Alexander Barroi, for the guidance, laughs, patience and freedom to develop my own work.

To Nils Nunold, for the cutting, polishing and sand-blasting of the substrates.

To Andreas Grunewald for the perfectly polished and etched samples.

To Richard Romanov, for the help with English translations.

To Jan Leschke, Benjamin Emde and Jörg Hermsdorf, for the laughs and company at the office during this whole year.

To Boris and Martha Rottwinkel, for really helping me to stablish in Germany.

To the OFT group, for the many laughs at our "*mahlzeit*".

To Volker Stoppe and Viola Merten, for the friendship and for offering their own house when I still had none.

To Armando Albertazzi Gonçalves Júnior, father and master, for the love, financial aid, motivation and inspiration.

To Suêde Albertazzi Gonçalves, mother, for the love, one year away from her little daughter.

To Deise Albertazzi Gonçalves, sister, for the company, love and friendship, unaltered by nothing more than an ocean between us.

To Adriano de Souza Pinto Pereira for the company, strength, laughs, talks, travels, for the many cooked dinners, for helping me becoming who I am today, for the love.

Resumo estendido

Diversas peças e ferramentas na indústria têm seu ciclo de vida reduzido devido ao atrito. Tecnologias de *cladding* (recobrimento) são comumente utilizadas para revesti-las com uma camada mais resistente. A utilização da tecnologia de *laser cladding* (recobrimento à laser) cresce devido às suas vantagens como diluição reduzida e menor deformação térmica em relação a outros processos de recobrimento. A opção de alimentação de arame – ao invés de pó – é cada vez mais utilizada, uma vez que o arame é mais facilmente armazenado, apresenta menor risco à saúde dos operários e desperdiça menos material no processo.

A tecnologia de *laser cladding* com alimentação a pó foi extensivamente estudada, mas, na literatura, a natureza do processo alimentado a arame ainda é pouco conhecida. Este trabalho visa analisar a influência dos dois principais parâmetros do processo – potência do laser e velocidade de avanço – sobre a geometria resultante em um único cordão de revestimento. A temperatura do substrato durante o processo também é analisada. São encontradas relações entre esses parâmetros e altura, largura e área do cordão de revestimento.

Finalmente, modelos analíticos são propostos a partir das relações previamente obtidas. O objetivo destes modelos não é uma descrição perfeita do processo, mas a obtenção de relações simples entre a geometria obtida e os parâmetros do processo, ainda que com algum erro. Estes modelos preveem a área, proporção entre altura e largura do cordão de revestimento, altura e largura do cordão de revestimento. Os modelos são então testados; suas exatidões, discutidas.

Abstract

Many tools and parts in the industry have a reduced life cycle due to wear. Cladding technologies are commonly used to apply a wear-resistant layer over them. The use of the laser cladding technology is increasing because of advantages such as reduced dilution and thermal deformations when compared to other cladding technologies. The wire feeding option – instead of powder feeding – is also increasing in the industry because of storage ease, increased health security and reduced waste of material.

The powder fed laser cladding was already extensively studied, but not much about the wire fed version of the process can be found in the literature. This work analyzes the influence of the two major process parameters – laser power and traverse speed – on the resulting geometry of a single cladding track. Temperature from the substrate during the process is also analyzed. Relations between those parameters and track height, width and area are found.

Finally, analytical models are proposed based on the relations previously obtained. The objective of those models was not to be a precise description, but simple relations between those process parameters and track geometry, even with some inaccuracy. The models predicted track area, height to width ratio, height and width. Models are tested; their accuracy, discussed.

Index

Symbology

A	*track area*	*mm²*
E	*energy per length unit rate*	*J/mm*
P	*laser power*	*W*
S	*traverse speed*	*mm/s*
S_W	*wire feed speed*	*mm/s*
V	*wire volume per length unit rate*	*mm³/mm*
c	*circle chord for track modeling*	*mm*
d	*distance from cross section to track's beginning*	*mm*
h	*track height*	*mm*
r	*circle radius for track modeling*	*mm*
t	*time*	*s*
t_i	*time instant correspondent to each cross-section location*	*s*
w	*track width*	*mm*
γ	*height to width ratio*	*-*

Chapter 1 Introduction

Laser cladding is a process where a laser beam melts an additive material on the surface of a substrate, creating solid metallurgical bond between them. The laser melts an area of the substrate's surface and the additive material, forming a molten pool. As it solidifies, the molten pool cools down with rates up to 10^7 K/s [1]. This process results on a functional layer over the surface of the substrate, improving properties such as corrosion and wear resistance [1]. In the industry, this process is mostly used for coating and repairing parts [2]. It has also great potential for rapid prototyping of cutting tools, dies, molds etc. [1,3], yet to be explored.

Comparing to processes such as electric arc or plasma welding, laser cladding presents lower dilution. Dilution is the mixing proportion of substrate and additive material [4]. When properly calibrated, only a very thin layer of the substrate is molten, keeping the functional properties of the added material. Furthermore, this process has more intrinsic advantages:

- Improved wear resistance [4,5]
- Reduced thermal distortion [2,4,5]
- Reduced post-cladding machining time and cost [4]
- Broad range of additive materials [2]
- Good for repairing parts [2,4]
- Ease to automate (powder feeding) [5]

Laser cladding has some disadvantages, such as high investment and maintenance cost [2,4]. Low electric efficiency of laser sources is also a known problem, decreasing the cost efficiency of the process [4]. Additional energy sources can raise efficiency and productivity of the process, as hot wire laser cladding, plasma heating and inductors.

1.1 Classification

There are three main types of laser cladding: powder bed, powder fed and wire fed [4]. These processes differ by the feeding method. Table 1-1 shows each process

type advantages and disadvantages. Wire fed laser cladding has a nearly 100% material usage efficiency, while a powder fed cladding process has a wide variety of usable materials [2]. The use of wire cladding processes is increasing also because of the ease of storage and the less health issues comparing to powder materials [2]. Further comparison of wire and powder feed regarding microstructure, material usage efficiency and surface roughness can be found at [6]. There is also research [7] currently investigating simultaneous deposition methods (both powder and wire fed).

Table 1-1: Attributes of laser cladding types [8]

	Powder-bed	Powder-feed	Wire-feed
Major advantages	Part complexity Accuracy	Material variety Part size	Deposition rate Material Quality
Major disadvantages	Part Size Material quality	Deposition efficiency Deposition rate	Part complexity Accuracy

Heralic [8] describes another three classifications for laser cladding with wire. If the wire spends too much time under the laser beam, it will melt before reaching the molten pool. Then, a drop forms on its tip due to surface tensions of the molten wire. This drop grows continuously, until gravitational forces detach it from the wire. Right after, another drop begins to grow. This phenomenon generates a track formed by spheres, characterizing the globular feed method.

When the wire is not molten before reaching the molten pool and is deposited on it while still in solid phase, plunging feed occurs. This method can generate good surface finish and small dilution, as shown by Kim and Peng in [9], but the process parameters need to be precisely tuned. If this is not the case, there is a possibility when the wire is not entirely molten, generating undesired surface finish and metallurgical bonding defects.

A smooth transfer occurs by melting the wire close to the molten pools surface, so that the molten metal is absorbed by the molten pool due to surface tensions. The most stable process is achieved by this method.

1.2 Scanner based laser cladding

Wire fed processes can yield to stability problems, generating cracks, pores or bad surface quality. Those problems occur e.g. when the wire oscillates out of the laser beam spot, what can be reduced by a scanner device (Figure 1-1).

A scanner is an optical device capable of deflecting the laser beam. It can either deflect it along a line with specific amplitude and frequency (1D) or over a pre-determined area (2D). The WZL laboratory of RWTH Aachen University investigated the use of a 2D scanner in laser cladding with wire [1,3]. Unfortunately, there is not much more research on this technology. A similar technique exists in arc welding. The electric arc can be deflected across the welding direction using a high frequency magnetic field oscillation [10], reducing penetration depth and increasing width of the welded clad. An oscillating beam creates the same effects.

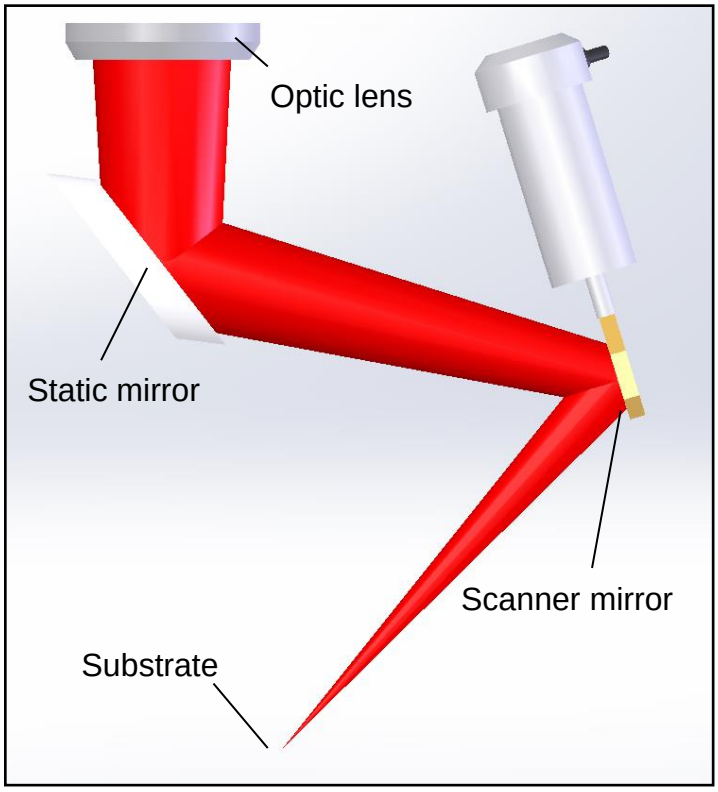

Figure 1-1: 1D Scanner device

Beam deflection over the work piece leads to a more homogenous heat distribution, diminishing wire misplacement problems and leading to clads with better finishing. Varying scan frequency and amplitude leads to different areas affected by the laser, therefore, to different geometries. Researchers achieved tracks from 1.52

mm wide by 0.63 mm high to 8.64 mm wide by 2.15 mm high with a 2D scanner [1]. On standard laser cladding, this range is otherwise only achieved with a large number of different and expensive optic elements, which would have to be changed during process. The use of only a single optic system reduces considerably time and cost of the process.

1.3 Geometry modeling

In additive manufacturing, achieving the desired track geometry is crucial. The right set of process parameters leads to a specific desired geometry. Thus, a proper relation between them needs to be found. Modeling the track geometric features based on the process parameters has been extensively studied on powder blown fed process. Finite element [11–13], experimental [14–17], analytic [18,19] and geometric [18–21] models have been proposed. Finite element methods will not be detailed.

Analytical geometry models can be proposed by different approaches. Cheikh [18] modeled the track upper section as a circle and calculated its center and radius based on the process parameters. Pinkerton [19] modeled not only the upper part, but both sections of the track as detached arc circles. After that, used mass and energy balance to define the boundaries of the molten pool, obtaining the track geometry. Both authors tested their models with experiments, obtaining good correlations.

Costa [14] found combined roles of different process parameters performing variable powder feed tests. With those values, he could predict height, dilution and track angle accurately. Oliveira [15] also performed some experiments relating combined parameters to the main clad dimensions, after calculating the required energy to melt separately substrate and additive material. The combined parameters found differed from each author, which was expected due to the results experimental nature. Oliveira and Davim [16] successfully established relations between process parameters and geometry features by multiple regression analysis. Saqib [17] proved that those relations can also be found by simple statistical methods on experimental data.

The track profile is important not only for laser cladding. When welding with consumable electrode gas-shielded pulsed-arc, the influence of the arc current and voltage on the track width, height and penetration depth is studied [22]. In the plasma

transferred arc welding technology, welding current, travel speed, powder feed rate etc. also influence track shape, motivating mathematical modeling [23].

Profile modeling in wire fed laser cladding also has its importance. There is, however, not much research on this topic. Syed and Li in [24] researched the effects of wire position, angle and direction on surface finish and geometry stability. In their study, front feeding with the wire tip near the molten pool's leading edge was the optimum setup. Kim and Peng in [9] studied the plunging method for laser cladding with wire, being able to stabilize it, obtaining solid bonding and good surface finish.

1.4 Accumulated heat influence

During laser cladding processes, it is natural for the workpiece to heat up. It happens mostly because of conduction transfers between molten pool and substrate [25]. With a hotter substrate, the existing thermal gradient is reduced, less energy is lost by the molten pool and its temperature increases. The extra energy leads to a bigger, deeper molten pool with higher dilution [25,26]. Ocylok's [26] results shows a preheating of 300°C increasing molten pool's size over 20%.

Heat also affects other characteristics of the clad. Many authors [27–31] studied the effects of preheating the substrate for powder fed processes. Costa [27] used simulations to demonstrate how the hardness of AISI 420 tool steel multi-layered clads depends on substrate's initial temperature and time interval between clads. Alimardani and Fallah [28,29] achieved crack-free coatings of stellite 1 with uniform microstructure by preheating a AISI 4340 steel substrate only locally. Jendrzejewski [30,31] successfully modeled temperature and stress fields of laser cladded stellite SF6 coatings on X10Cr13 chromium steel, relating higher initial temperatures to less cracking.

There are fewer studies on the heat influence in wire fed laser cladding processes. Kim and Peng [32] concluded that the depth and dilution of a clad layer are much bigger at the end of a track than on its beginning. They also discovered that the molten pool width increases with temperature, but the track width above the surface level remains almost constant on their experiments. The effect of molten pool enlargement was also studied by Hofman [33], where he was able to control dilution,

based on molten pool width. Accordingly to his studies, dilution remains low as long as the molten pool width stays less than 90% of the beam spot diameter.

1.5 Document structure

The first chapter of this work presented the actual state of the art of the scanner-based wire fed laser cladding technology. The next chapter defines and motivates this work. Chapter three details the setup used for cladding the tracks. The forth chapter explains how the experiments were designed. It also describes the procedure from cladding the track to obtaining cross sections. Then, the fifth chapter shows the results obtained. Its first section explains the behaviors of the temperature measurement, while its further sections try to correlate the geometrical dimensions measured with the process parameters. On the sixth chapter, three different models for geometrical features of the track were proposed and tested. Their results and accuracy are discussed. On the last chapter, all the conclusions obtained on this work are discussed.

Chapter 2 Problem definition

In the industry, wear has always been a constant factor shortening the life cycle of tools and parts. Thus, it is desirable to increase their wear resistance. Building parts entirely of a noble, wear resistant material is not always financially viable. A solution is to produce hybrid pieces: a noble material coating over a base, cheap one. The coats can be applied using laser cladding process.

To produce those layers, tracks are cladded overlapping each other laterally. A flat, wide geometry is often desirable, once they generate less error when overlapping. It is also important that they have a constant geometry along their lengths to produce a uniform layer.

This geometry, however, presents deformations along the track, tending to be flatter and wider on its end. These variations originate from the accumulation of heat in the process. As the laser beam interacts with the substrate, it absorbs energy, heating up. A hotter molten pool grows larger, resulting in several track changes.

This work aims to investigate the relation between the two major process parameters – laser power and traverse speed – and track geometry for different operation points. Models to relate these process parameters and the geometrical variation were proposed.

With those results, the process can be better understood. Knowledge makes controlling it possible. With more constant tracks, it is possible to produce better quality layers, therefore, better parts.

Chapter 3 Experimental setup

As the name suggests, scanner-based wire fed laser cladding processes are complex. A wide range of variables influence the final track geometry obtained. Those main variables are described in section 3.1. On section 3.2, the setup of the system used is detailed.

3.1 Process parameters

A large number of variables affects scanner-based wire fed laser cladding processes. When these variables are controllable, they are parameters. The four main parameters are laser power, wire feed speed, scanner amplitude and traverse speed. Each one has a unique effect on the process.

- **Laser power [W]** – determines the maximum energy input, having the strongest impact on dilution and penetration depth.
- **Traverse speed [mm/s]** – determines both the amount of added material per length unit and input energy per length unit. Affects heat propagation, therefore track geometry.
- **Wire feed speed [m/s]** – strongly related to track height. Multiplied by wire cross section area, determines the volume of added material per time unit. It is also possible to obtain the mass of added material per time unit by including wire density on the equation.
- **Scanner amplitude [mm]** – strongly affects track width, controlling the molten pool shape. Has a strong effect on penetration depth and dilution. When the scanner amplitude is varied, interaction with the oxides on the surface also changes, affecting surface finish.

Besides its power, the laser beam has other parameters that also influence track geometry. None of them has such a strong effect, but if neglected, results can diverge from expected.

- **Laser to substrate angle** – influences reflection of laser beam, therefore energy absorbed. Absorption is optimal at 90°.

- **Laser beam spot size and energy density** – affects molten pool shape and depth.
- **Laser wavelength** – different wavelengths are absorbed differently by metals. An optimal wavelength can reduce considerably required input energy by raising absorption efficiency.

Other parameters of the scanner device also influence track geometry and must be tuned.

- **Scanner frequency and waveform** – influence mainly the final shape of the track surface.

A wrong choice for wire position can also affect track surface finish and metallurgical bond. The two parameters bellow also should be tuned.

- **Wire to substrate angle** – influences how the wire is melted, changing material transfer kinds (globular, smooth or plugged). Process stability strongly depends on this parameter.
- **Wire tip distance to center of laser beam spot**
    - **Parallel to cladding direction** – changes how long the wire stays under the laser beam before reaching the molten pool.
    - **Perpendicular to cladding direction** – controlled by scanner device. In order to keep stability, the wire tip must stay within laser beam spot.

To protect the hot, newly-cladded surface from oxidation, it is important to isolate it from atmosphere. An inert gas is blown over it before, during and after the process for this purpose. Gas type and flow rate also contribute on surface finish quality.

3.2 Setup description

The system consists on a laser head, a scanner device, a wire feeder, a pyrometer and a NC (Numerical Command) machine. Each of these elements is described on the following sections. Figure 3-1Figure 3-1: Laser cladding system. 1: Laser head. 2.1: Static mirror. 2.2: Movable mirror. 3.1: Wire torch. 3.2: Wire feeder pusher. 4: Pyrometer.

shows a schematic (left side) and a photo (right side) of the actual system, with identifications of each component. The NC machine is not identified on this figure, but it holds this assemble on its Z-axis.

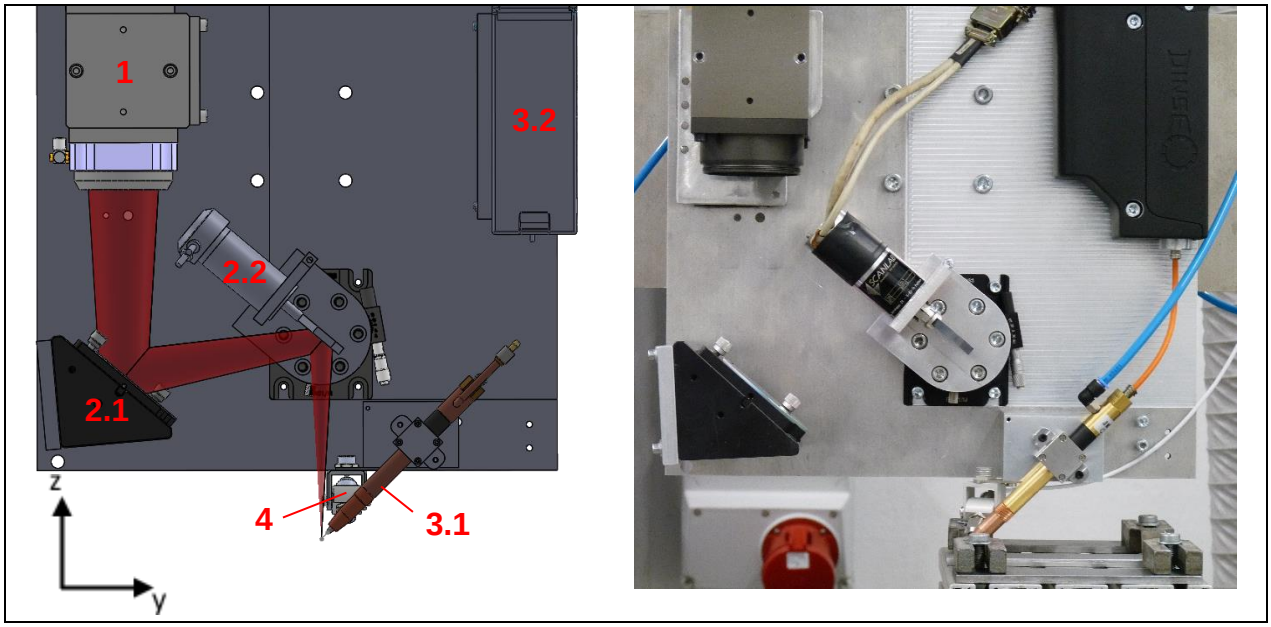

Figure 3-1: Laser cladding system. 1: Laser head. 2.1: Static mirror. 2.2: Movable mirror. 3.1: Wire torch. 3.2: Wire feeder pusher. 4: Pyrometer.

3.2.1 Laser source

The laser source used is a diode laser head (component 1, Figure 3-1) of 1032 nm wavelength. Its maximum power is 2200 W. Focal distance is of 400 mm.

3.2.2 Scanner system

To deflect the laser over the substrate, a scanner system is used. It consists of a pair of mirrors, one static and one movable – named as scanner mirror. On Figure 3-1, the static mirror is identified as 2.1, while the movable mirror is the component number 2.2. The static mirror reflects the laser beam to the movable one. Then, the movable mirror deflects the beam to the substrate. A signal generator is used to set the movement of the movable mirror. The maximal angle that this scanner can deflect is of 19.5 radians. As a maximum angular speed, it moves 1% of its maximum angle in 0.8 ms, and 10% in 2 ms.

3.2.3 Wire feeder system

The wire feeder used is a DINSE® system. On Figure 3-1, the component 3.1 represents the wire torch, while 3.2 is the wire feeder pusher. It has the functionality to measure the real wire speed of the process. Its maximum wire feed speed is of 333.33 mm/s (or 20 m/min).

3.2.4 Pyrometer

To acquire temperature data, a $\mu\varepsilon$® CT SF22 pyrometer was used, represented as 4 on Figure 3-1. This pyrometer has a temperature range of -50°C to 975°C, with an uncertainty of ±1°C. It measures wavelengths between the range of 8 to 14 µm, with a focus diameter of approximately 6.5 mm. The pyrometer was focused 10 mm away from the laser focus spot, as vertical as possible to minimize reflections.

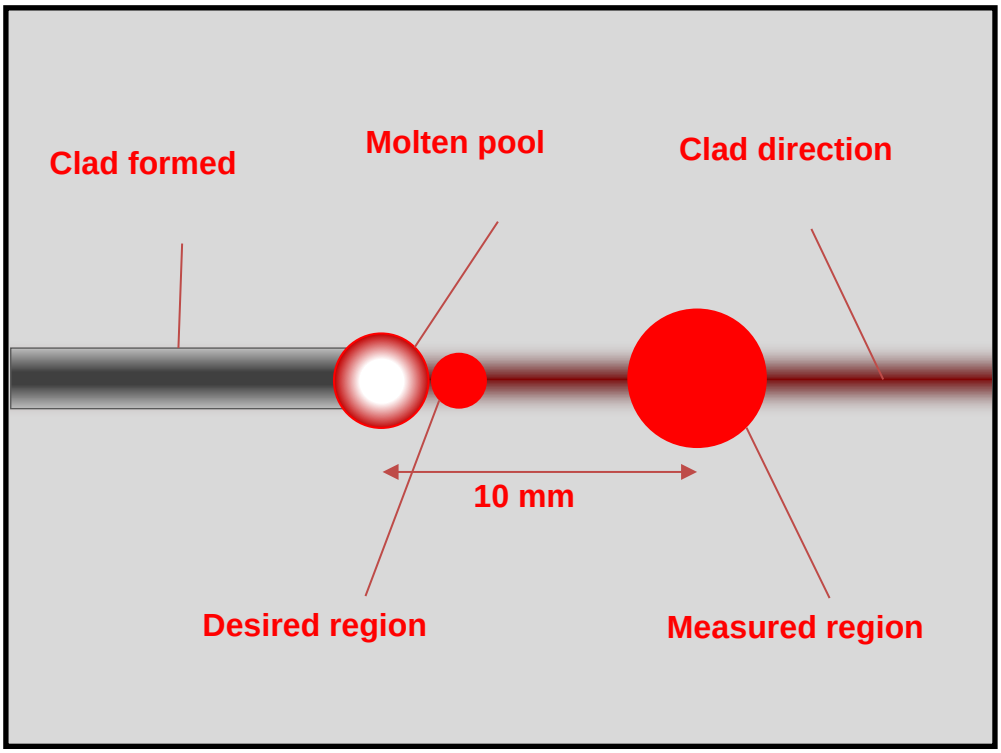

Figure 3-2: Regions of desired and measure temperatures. Measured region is larger and further away from the molten pool than the desired one.

It is desirable to measure the temperature right ahead of the molten pool. This region, however, is not measurable with this setup due to reflections from the molten pool. It is also desirable to acquire temperature from a smaller spot on the substrate,

which is not possible with the current pyrometer's optics. Figure 3-2 illustrates the desired and the measured regions.

As temperature is measured away from the molten pool, an error appears. Heat does not travel instantly on the substrate, leading to a delay on the measured data. This delay is not constant – different laser powers and traverse speeds change its duration. The effect is further discussed on the experiment setup chapter.

The pyrometer recording is turned on right after the start of the NC program. It keeps recording temperature after the process ends until it reaches around 25°C, when it is shut down.

A laser pointer was used to calibrate the pyrometer position. Figure 3-3 specifies the point measured by the pyrometer.

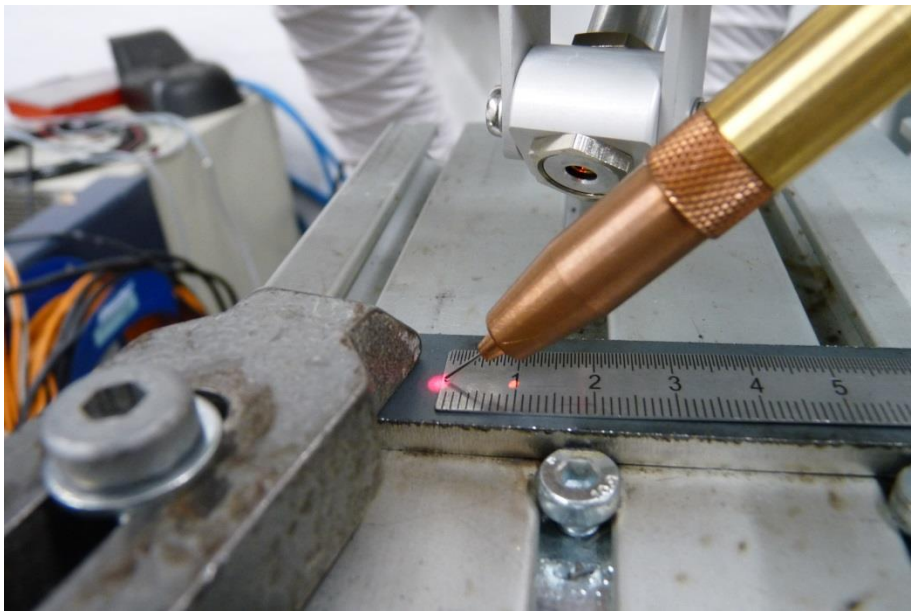

Figure 3-3: Pyrometer position calibration with the laser pointer

3.2.5 Numeric controlled machine

A 3-axis NC machine was used to control the system. The g-code used was programed to perform the following tasks:

- Turn on protection and scanner movable mirror cooling gases.
- Wait 5 seconds.
- Turn on the wire feeding system.
- Turn on the laser beam.
- Move the substrate with a desired traverse speed along 60 mm.
- Stop the wire feeding.
- Move with the same traverse speed 2 mm to cut the wire with the laser.
- Turn off the laser.
- Move more 3 mm and stay still in position.
- Wait 2 seconds.
- Turn off the gases.
- Turn off the machine axis system.

Chapter 4 Experimental

To comprehend more of the process behavior, it is a necessity to study the influence of laser power and traverse speed on track geometry. To do so, experiments were designed, shown on section 4.1. Further sections of this chapter describe other information about the setup and about standard procedures stablished to acquire cross sections.

4.1 Design of experiments

Track geometry depends highly on laser power and traverse speed. The laser power affects directly the molten pool's temperature. A hotter molten pool grows larger, deeper and has lower viscosity, flattening and widening the track profile. Traverse speed also influences track geometry. If the beam travels faster across the substrate over the same 60 mm, the total amounts of energy absorbed and wire fed decrease. Because of this reduced energy, temperature increases less – also leading to a flatter and wider track – but, due to the reduced total volume of added wire, track area becomes smaller. Tracks usually present geometrical variations along their lengths. As soon as the laser beam generates a molten pool on the substrate, its temperature raises. With the increase of temperature, track geometry becomes flatter and wider. As those geometrical changes originate from temperature, they also depend on these process parameters.

Of all process parameters, laser power and traverse speed have the strongest influence on track geometry. Therefore, those are the parameters studied on this work. Remaining parameters are set to constant values selected from previous experiments.

Table 4-1 represents the planned experiments. The team currently working on this project designed the shape of this table, while the process parameters values were obtained on previous experiments performed by the author.

On this table, the numbers from 1 to 17 identify each experiment. Laser power values where chosen to cover a range of values that proved functional on previous experiments. Their laser power step is an arithmetic progression of 3% of the maximum laser power (2200 W). The traverse speed range, however, was chosen differently.

The higher and lower values were obtained experimentally, assuring the stability of the process. For defining the intermediate values, a geometric progression was made.

Table 4-1: Experiments table

		Traverse Speed [mm/s]						
		0.83	1.15	1.60	2.20	3.05	4.22	5.83
Laser Power [W]	968	15			10			17
	902				9			
	836				8			
	770	4	3	2	1	5	6	7
	704				11			
	638				12			
	572	14			13			16

On the experiments 1 to 7, laser power is constant while traverse speed varies, in order to isolate this parameter's influence on track geometry. The experiments 8 to 13 aim to analyze laser power influence on those geometrical variations. Finally, experiments 14 to 17 represent the limit values of this operational window, where both parameters are varied. Unfortunately, those tests were performed only once due to the limited time available at the workstation. If those tests were performed two more times, a more reliable result would have been achieved.

During the process, the pyrometer records substrate's temperature. The pyrometer focus is 10 mm ahead of the laser, on the direction of cladding, as explained on section 3.2.4.

Initial temperature remains between 25°C and 30°C. Each track is performed on a different substrate to prevent most of the heat to accumulate. After cladding, time cools down the NC machine's temperature to room temperature. A new track is cladded only after this cooling down interval.

Once all tracks are cladded, they are cut transversally to clad direction. The cross sections are photographed, and width, height and track area, measured. More details of the cutting and measuring procedures are respectively on sections 4.4 and 4.5.

After obtaining cross sections dimensions, the geometric variations in each track and between them are analyzed. Relations between this variation and the

process parameters are studied. Finally, models are proposed to predict the geometry from the experiments 14 to 17, where both influences are present. Discrepancies are measured and discussed.

4.2 Constant setup parameters values

As only laser power and traverse speed vary, it is necessary to set constant values to the remaining parameters. The wire used was a 318 Si with a diameter of 0.6 mm and density of 8 mg/mm³. Its feed speed is set to 10 mm/s, which gives an 11.31 mm³/s wire volume input. To control the scanner device, the signal generator emits a 50 Hz triangular wave with amplitude of $0.15V_{pp}$, oscillating the laser beam along a line approximately 1.125 mm long. The laser beam focuses on the substrate almost perpendicularly to it. The scanner mirror is used to position the wire tip on the leading edge of the laser beam, keeping the laser beam from being precisely perpendicular to the substrate. Argon is used as the protection gas, blown at 5.4 l/min (room temperature).

4.3 Workpiece preparation

The S235 mild steel workpieces were laser cut to 100 mm by 20 mm blanks, an adequate size for the process. Afterwards, they were sandblasted to remove oxides and impurities from surface.

4.4 Cross sections

To obtain cross sections, the workpieces needed to be cut. Aiming comparability for the acquired data, standard cutting procedures were established.

In order to acquire as many data as possible, the tracks were cut seven times perpendicular to cladding direction, as shown of Figure 4-1. The first cross section obtained is 5 mm away from the beginning of the track. The next two cuts are spaced 5 mm from each other. Further cuts are spaced by 10 mm. The cuts were not precisely made on these positions due to the disc saw used. Errors have an estimated maximum magnitude of ± 0.5 mm.

The smaller spacing on the beginning is required as this region presents the highest temperature gradients, furthermore the highest geometric variation.

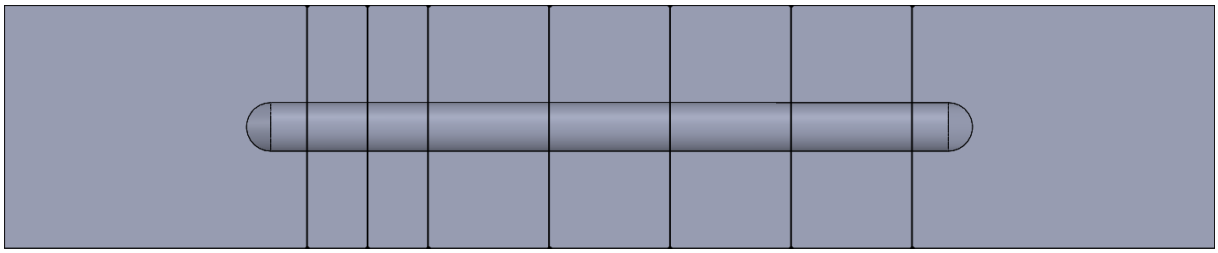

Figure 4-1: Cut pattern for the tracks performed. Seven cross sections are obtained from each track.

After cutting the pieces, the cross sections were polished, etched and photographed in the direction of cladding, e.g. facing the end of the track.

4.5 Measurement description

Quantifying the geometrical variations on the tracks requires the cross section images to be measured. To do so, a straight line is defined as the division between clad and substrate on substrate surface. This procedure was performed using an image measurement software. After that, the image is measured to obtain the following dimensions. They need precise definitions to be comparable in all the experiments. Their formal descriptions are bellow and they can be seen on Figure 4-2.

- **Clad width [mm]:** largest track dimension that is parallel and either above or on the substrates surface, delimited by the division line.
- **Clad height [mm]:** largest clad dimension that is above and perpendicular to the substrates surface, delimited by the division line.
- **Track area [mm²]:** cladded area above the division line. This area was measured by using a contour tool of the same image measurement software.

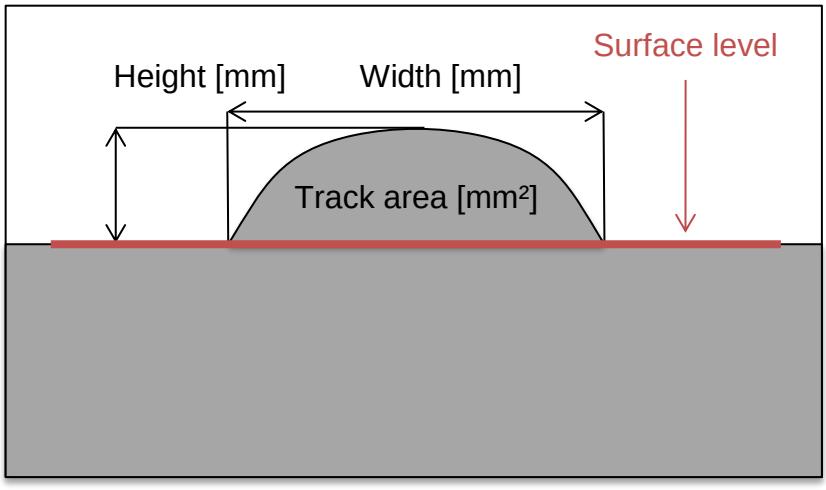

Figure 4-2: Geometric parameters description

Chapter 5 Results

On this chapter, the results are presented. On section 5.1 the temperature data acquired by the pyrometer is studied. On section 5.2, all the geometrical dimensions are presented; their relations with the process parameters, analyzed.

5.1 Pyrometer data

During the process, the pyrometer recorded the temperature from a region 10 mm ahead of the molten pool, on the direction of cladding, with 0.1s of sample time. Acquired data follows the model on Figure 5-1 bellow. The divisions on the picture are explained on further sections.

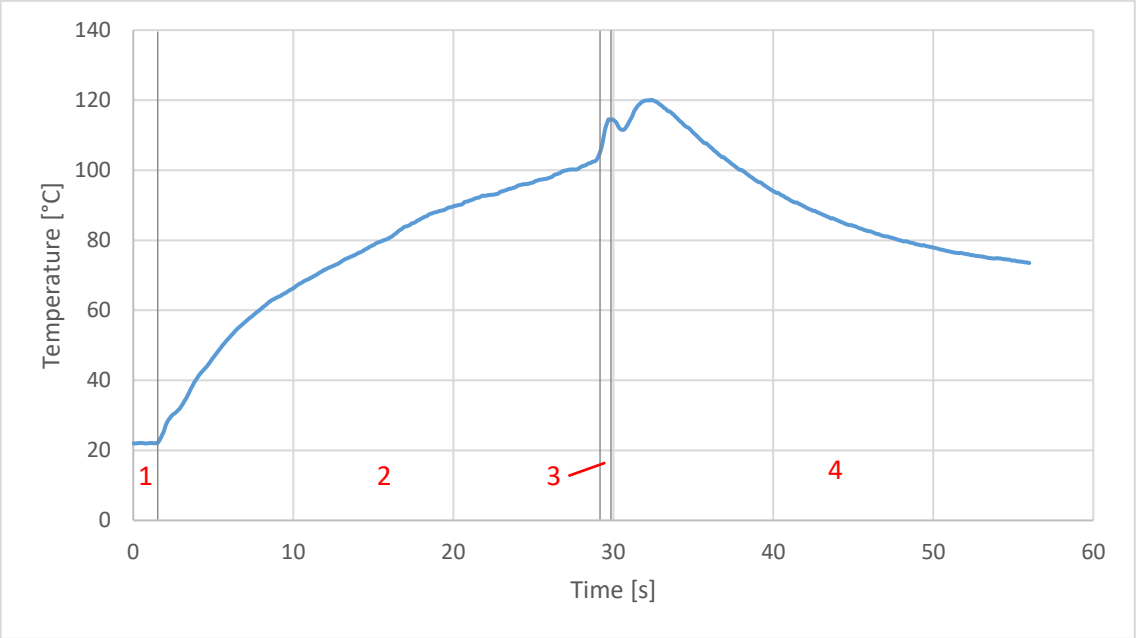

Figure 5-1: Temperature data from track 1 – 770 W and 2.20 mm/s

5.1.1 Section 1 – Before the process

This section represents the temperature not affected by the process. The process itself, however, starts on this section. Because of the 10 mm distance between laser beam and pyrometer foci, the process starts before the pyrometer detects any temperature variation.

This delay is not constant. Faster traverse speeds reduce the relative speed between laser beam and the isotherms from the molten pool, resulting on a higher delay. If the temperature of the base of the NC machine is higher – what happened due to the cladding of consecutive tracks, even with the cooling down interval – heat sinking from substrate to the NC machine reduces, heating up the substrate faster and shortening the cited delay.

5.1.2 Section 2 – During the process

This section represents the temperature that was affected by the cladding of the 60 mm long tracks. Its beginning is on the last recorded temperatures sample that is at room temperature. At room temperature, temperature oscillations do not exceed a ±0.1°C range. When the pyrometer measures a variation bigger or equal to 0.3°C, it defines the beginning of this section. On the example on Figure 5-2, the signalized sample at 1.5 s and the one that follows it have a difference of 0.5°C.

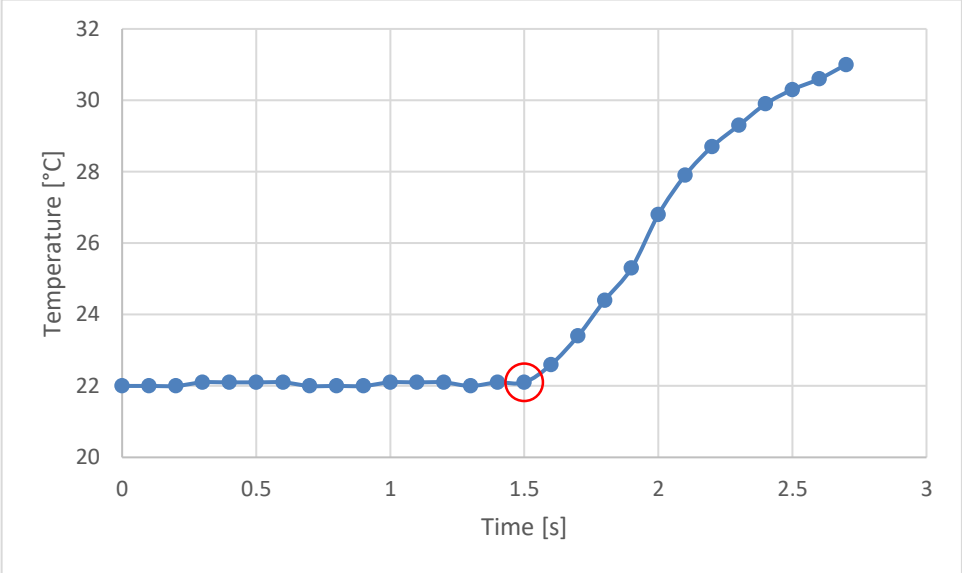

Figure 5-2: Limit sample between sections 1-2 for track 1. This sample is the beginning of section two, belonging to it

Because of the same delay effect described on section 5.1.1, the cladding process of all tracks also ends before the end of this section. Its end is calculated as 60 mm away from its beginning, based on speed and time, as calculated in *(1)*.

$$t = \left(\frac{60}{S}\right) + t_0 \quad (1)$$

Where t stands for the calculated end time, S stands for traverse speed and t_0 stands for this section's initial time. However, this limit is not a precise value. As temperature at the end of this section is different from the one at its beginning, the delay can vary. Figure 5-3 shows the calculated end sample for this section.

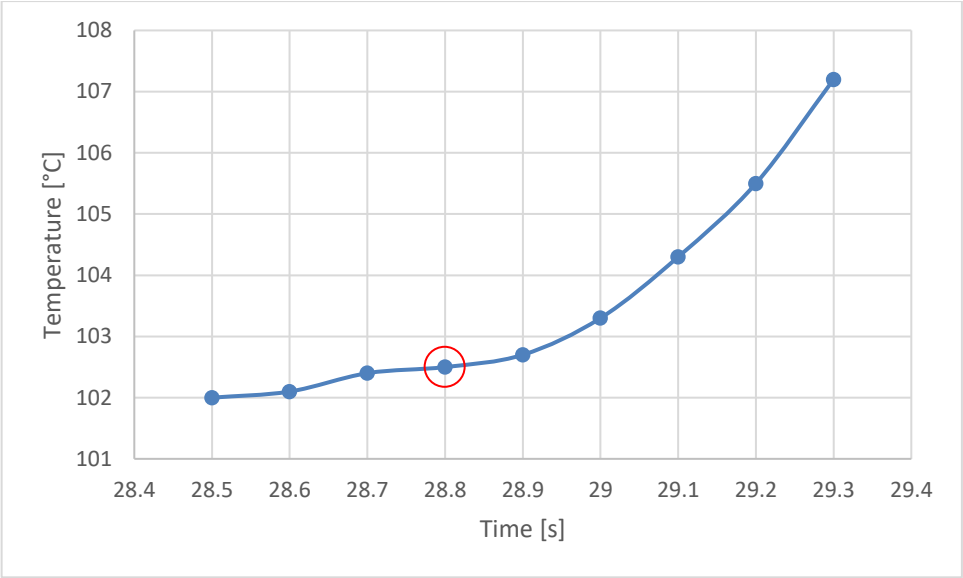

Figure 5-3: End of section 2. The marked sample delimits the end of section two, belonging to it.

This section corresponds to the temperature measured during the cladding process. To relate it with track geometry, temperatures on the cross sections locations need to be identified. It is done by calculating the corresponding time for the cross section positions, as done in *(2)*.

$$t_i = \frac{d_i}{S} \qquad d_i = \{5\ 10\ 15\ 25\ 35\ 45\ 55\}\ mm \qquad i = \{1\ 2\ 3\ 4\ 5\ 6\ 7\} \tag{2}$$

Where t_i stands for the calculated time for each cross-section, d_i stands for the distance between each cross section and the beginning of the track that is parallel to clad direction and S stands for each track's traverse speed. Cross section temperature is than defined as the temperature at that instant.

5.1.3 Section 3 – Wire cutting

After cladding the 60 mm long track, the NC program stops the wire feeding and continues the cladding movement for 2 mm more. As the laser is on during this interval, it cuts the wire. With no more material added, more energy from the laser beam enters

the molten pool, increasing its temperature faster. At a traverse speed of 2.20 mm/s, this 2 mm distance is covered in 0.9 seconds. Figure 5-4 represents this section.

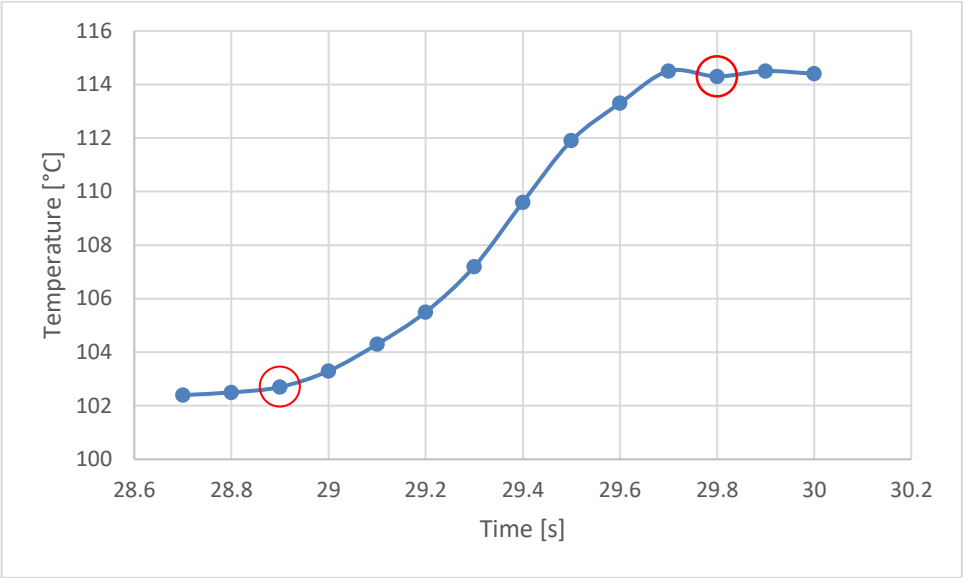

Figure 5-4: Section 3 with its limit samples. Time duration of this section is 0.9s.

The section is 0.9s long, starting right after the end of section 2. Again, this is not a precise limit because of the already cited delay.

5.1.4 Section 4 – Laser shut off

With the wire cut, the NC program shuts the laser off and continues the cladding movement for 3 mm more at the current traverse speed. Then, it stands still. This section starts on the first sample after the end of section 3. Temperature oscillates on the beginning of this section, and then, temperature gradually decreases as the track cools down. The explanation for the oscillations follows.

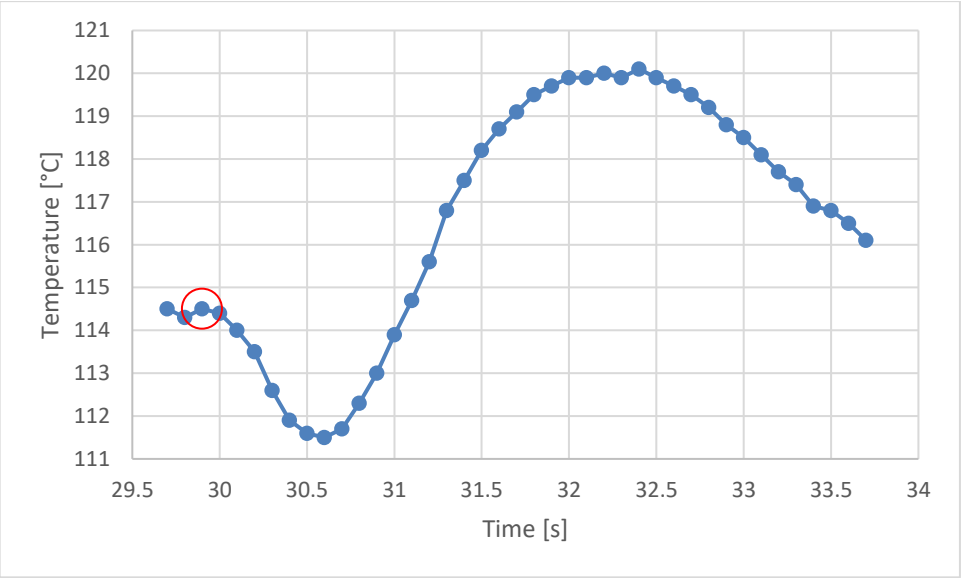

Figure 5-5: Beginning of section 4. Marked sample belongs to this section.

The temperature oscillations consist on a decrease, an increase and another decrease of temperature, as seen on Figure 5-5. At the beginning of this section, laser is shut off. The cease of energy input explains this first decrease. Then, as the axis stop, more isotherms travelling from the molten pool reach the region measured by the pyrometer, making it record an increase on temperature. After that, temperature decreases until the end of the measurement. It continues to cool down until it reaches around 25°C.

One sample has a bigger importance on this section. When the axis movement stops, the temperature measured by the pyrometer instantly reduces its decrease. The sample at 30.3s is this inflexion point. The graphs on Figure 5-6 highlight this point. It makes predicting the instant where the process started possible. On the case of track one – at 2.20 mm/s – the process started 28.2 seconds before that instant. Figure 5-7 shows the temperature curve without the estimated delay of 0.8 s.

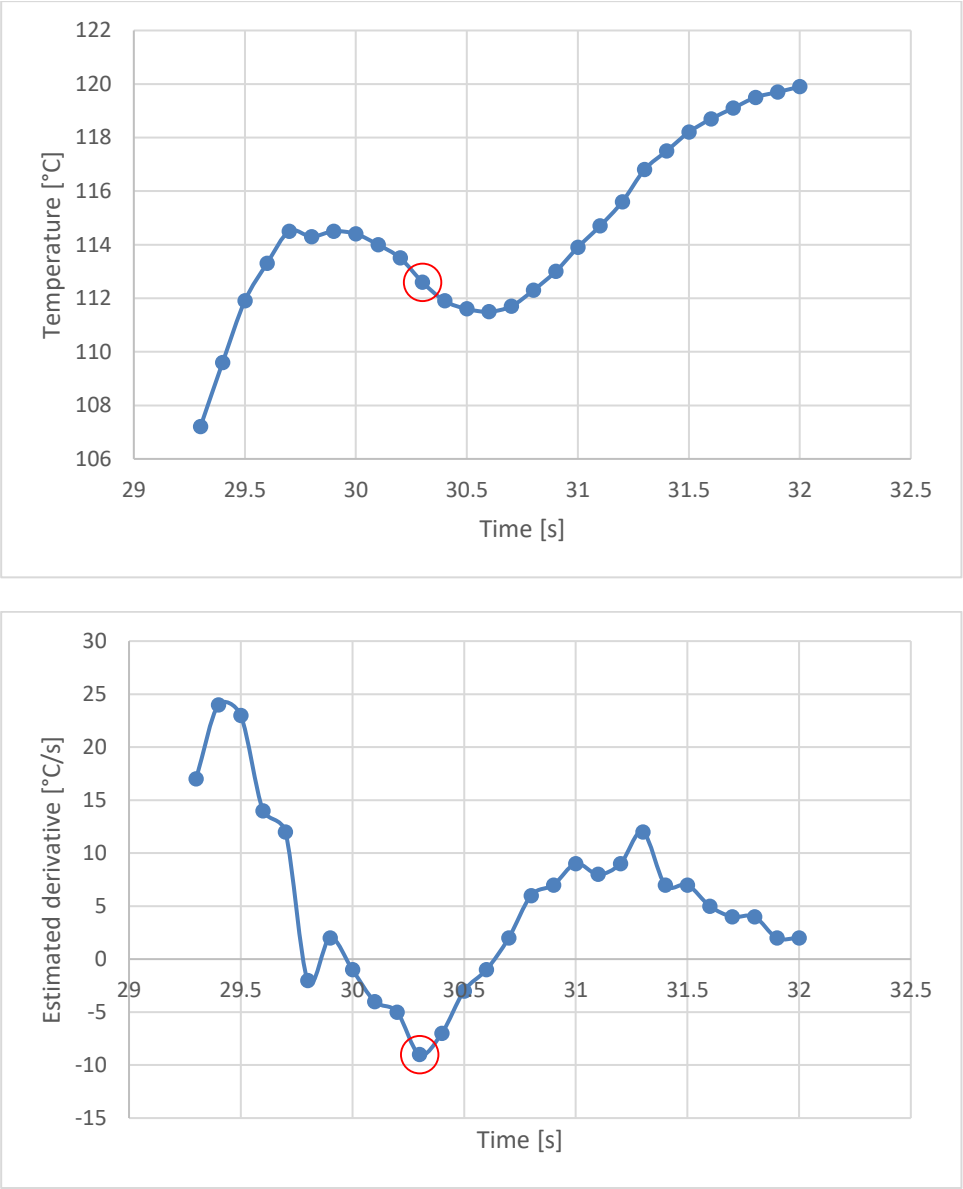

Figure 5-6: Inflexion point on temperature curve (top graph). The inflexion point is a valley on the estimated derivative curve (bottom graph).

The curve in Figure 5-7 estimates the instants where each event happened at the pyrometer's desired measurement spot (on the leading edge of the molten pool). Temperature magnitude, however, does not match. It increases exponentially when closer to the molten pool. With the current setup it was not possible to determine the real temperature. A second pyrometer, an IR camera or a pyro camera would have been useful for that purpose.

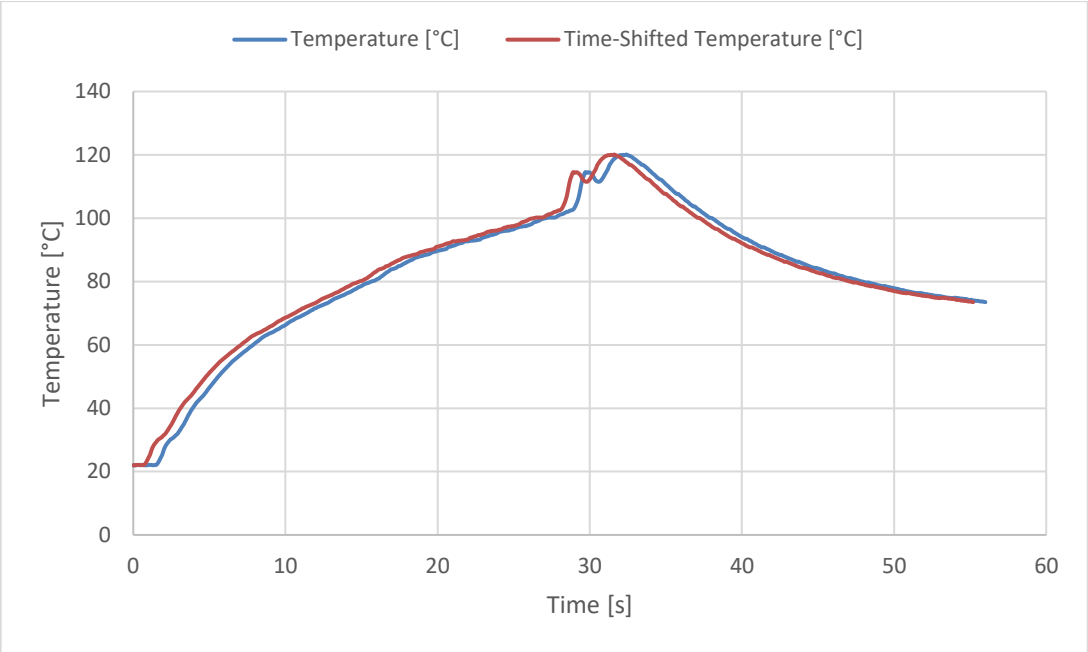

Figure 5-7: Time-shifted temperature curve. This curve begins at the estimated process start point.

5.2 Data analysis

The tracks were designed, cladded, cut, photographed and measured. Here, they are separated in two groups to analyze each parameter influence individually. When analyzing traverse speed influence, laser power was kept constant. Tracks with constant traverse speed were analyzed for the laser power influence study. Later, all tracks are analyzed together in order to investigate the complete geometry variation behavior along the whole process operational window.

5.2.1 Traverse speed influence on temperature

Laser power was kept constant to 770 W while traverse speed varied from 0.83 mm/s to 5.83 mm/s, as described on section 4.1. Temperature was recorded at the distance of 10 mm ahead the laser beam on the direction of cladding, as described on section 3.2.4. Recorded data for those tracks are on Figure 5-8 bellow.

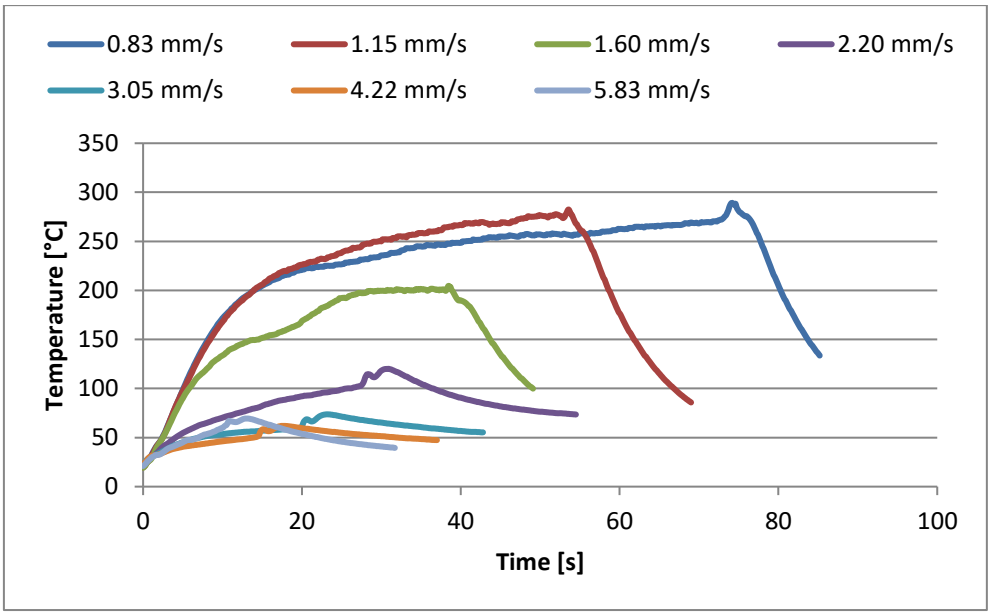

Figure 5-8: Temperature records for tracks performed.

On this graph, it is visible that temperature increases faster on the beginning of the slowest tracks (1.60 mm/s and slower). As the beam moves slower over the substrate, the hotter, slower isotherms from the molten pool reach the spot measured by the pyrometer quicker, leading to this faster heating record.

The distance between the molten pool and the pyrometer measurement spot also has strong impact on the obtained data. As the pyrometer cannot focus directly the leading edge of the molten pool, the non-instant propagation of heat on the substrate affects its recording. On tracks faster than 1.60 mm/s, the laser beam and the pyrometer travel faster than the hotter isotherms from the molten pool through the material. It slows the temperature rising of the measured data. Thus, the post-increase of temperature explained on section 5.1.4 happens once hotter isotherms reach the pyrometers measured spot. Figure 5-8 shows this post-increase on the tracks faster than 1.60 mm/s.

There is an unexpected behavior on the fastest track: it is hotter than it should. There was a wire misplacement on the beginning of this track – it was too far away from the substrate. As the wire took a longer time to enter the molten pool, the whole substrate became hotter. This mistake is on the left side (beginning) of this track's surface, on Figure 5-9.

Figure 5-9: Track surface cladded with 770 W, at 5.83 mm/s. There is a region without wire on the beginning (left), created because the wire was placed too far away from the substrate.

The track cladded with the slowest speed also shows a curious effect: the recorded temperature is actually lower than it should. Because this track is obtained by the slowest speed, it presents the biggest amount of cladded material. The added material on this track retains part of the heat. This oversized track shields the substrate from the heat. However, the peak generated when the axis stop (explained on section 5.1.4) is the hottest. As the total energy input on this track is the highest, it still has the hottest molten pool.

Figure 5-10: First cross sections of the track obtained at 0.83 mm/s (left) and at 1.15 mm/s (right). Volume of the track at the left is the biggest, explaining this shielding effect.

Both of those effects can be seen on Figure 5-11. It shows how temperature behaved for different traverse speed values. Each color represents one track, and each point, the temperature measured on specific spots during the process (5, 10, 15, 25, 35, 45 and 55 mm from the beginning of the track). These are the same locations from where the cross sections were obtained. It is visible that, for the tracks obtained at speeds lower than 3.05 mm/s, the lowest temperature rises when decreasing traverse speed. This is expected due to the higher amount of energy transferred to the substrate from the beginning of the track until this point (5 mm away). Its calculation is in *(3)*. Table 5-1 presents its results.

$$E[J] = \frac{d[mm] * P\left[\frac{J}{s}\right]}{S\left[\frac{mm}{s}\right]} = \frac{5 * 770}{S}\left[\frac{J * \frac{mm}{s}}{\frac{mm}{s}}\right] = \frac{3850}{S}[J] \quad (3)$$

Where E stands for energy, d stands from each cross section distance from the beginning of the track, P stands for laser power and S for traverse speed. Values were calculated based on equation *(3)*.

Table 5-1: Energy emitted from the laser source on the first 5 mm of each track.

Speed $[mm/s]$	0.83	1.15	1.60	2.20	3.05	4.22	5.83
Energy $[J]$	4622	3348	2406	1750	1262	913	660

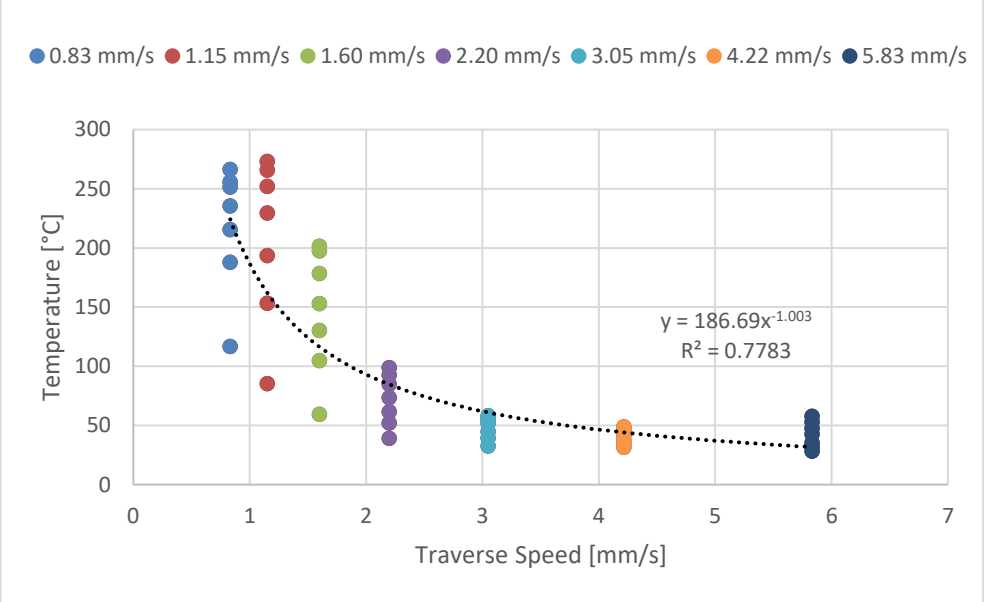

Figure 5-11: Traverse speed influence on temperature variation for each track.

Figure 5-11 shows that temperature measurement varies only a few tens of degrees on the tracks obtained with the highest transvers speed, but over 150°C on the two lowest ones. Again, the main reason for that is the higher amount of energy transferred to the substrate on the slower tracks.

Eventually, when temperature reaches a level where the energy input is the same as the energy dissipated, temperature would stabilize. A 60 mm long track, however, is not long enough to reach this level for the current sets of parameters.

5.2.2 Traverse speed influence on track geometry

From the cross section images, track geometry was measured accordingly to the procedure described on section 4.5. Now, each geometric characteristic is described; their relations, discussed.

5.2.2.1 Height

The values obtained for track height are on Figure 5-12. The colors represent tracks cladded with different traverse speeds, and the points, heights measured from respective cross sections.

Height varies differently for each traverse speed. Especially for slower traverse speeds, track's end is flatter than its beginning. On the speed of 0.83 mm/s, the final height is 87% of the initial one. This happens because, for low speeds, the thermal gradients on the substrate are bigger. As temperature grows, the molten pool gets larger [26]. A larger molten pool lets the molten metal flow in a wider area before it solidifies, leading to flatter and wider tracks. Figure 5-13 shows the decrease of height along each track due to the temperature increase. On the three faster tracks, however, this effect is not noticeable. There is no relevant deformation, as the temperature does not raise enough for that.

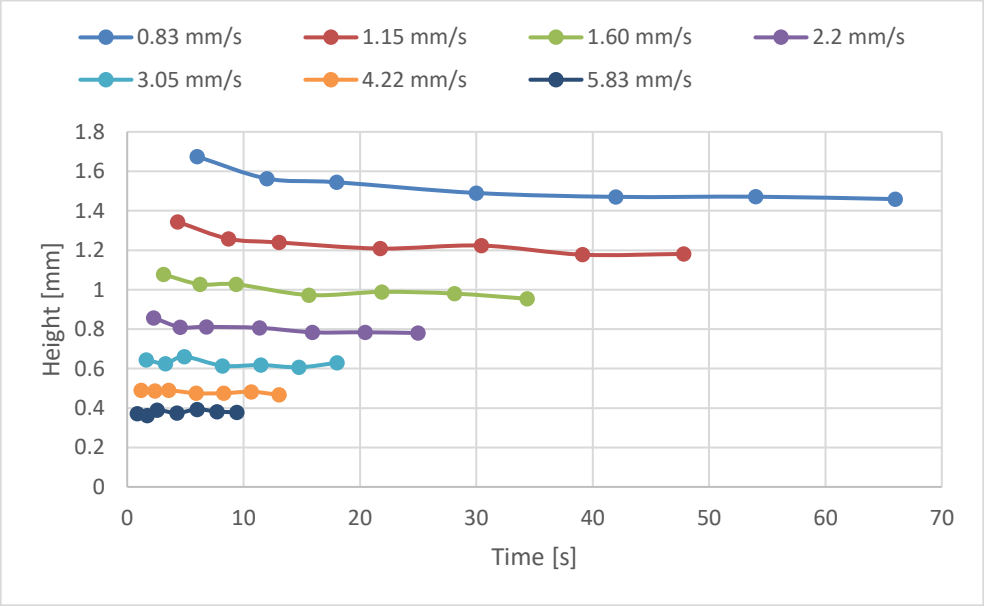

Figure 5-12: Height values of cross sections for each track.

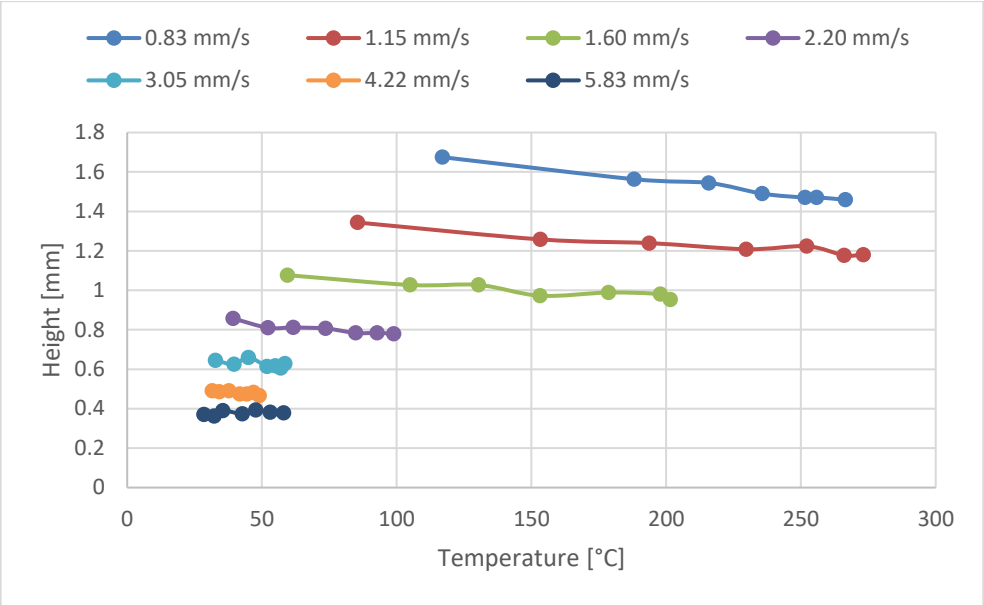

Figure 5-13: Height decrease along tracks due to temperature increase.

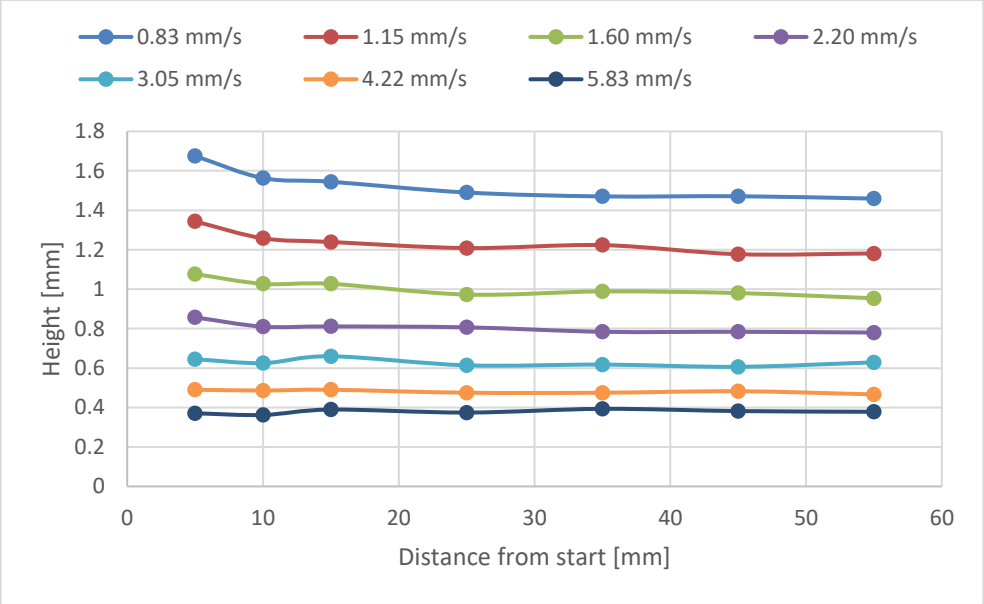

Figure 5-14: Height values of cross sections for each track relating to their position.

The influence of traverse speed on height values is strong. There is an almost constant offset between tracks, which increases when traverse speed decreases. This effect is easily seen on Figure 5-14. For an increase in speed of 700% (0.533 mm/s to 5.83 mm/s), the final height of the tracks decreases by 74%. Wire misplacement on faster track does not interfere on measured height values. Because of this effect, it is hard to establish a relation between height and temperature.

This decrease on height happens because the amount of material deposited on the slower tracks is larger. This effect can be quantified by calculating the volume of

added material per length unit, which is considerably higher on slower tracks. Its calculations are on (4), and its results, on Table 5-2.

$$V\left[\frac{mm^3}{mm}\right] = \frac{S_W\left[\frac{mm}{s}\right] * \frac{\pi * {D_W}^2[mm^2]}{4}}{S\left[\frac{mm}{s}\right]} = \frac{10 * \frac{\pi * 0.6^2}{4}}{S}\left[\frac{mm^3}{mm}\right] \quad (4)$$

Where V stands for added material volume per length unit, S_W stands for wire feed speed, D_W stands for wire diameter and S stands for traverse speed.

Table 5-2: Material volume per length unit for each track

Speed $[mm/s]$	0.83	1.15	1.60	2.20	3.050	4.22	5.83
Material volume per length unit $[mm^3/mm]$	27.14	19.63	14.19	10.26	7.42	5.36	3.88

Figure 5-15 shows how strong this relation is. Correlation coefficient is $R^2 = 0.99$ for a potential function, meaning a direct relation between these two factors.

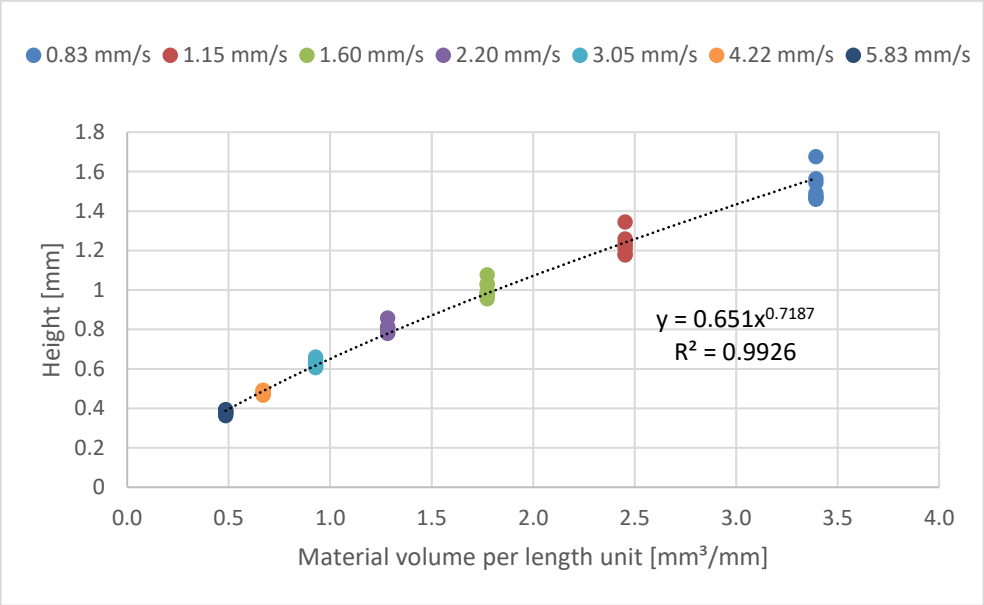

Figure 5-15: Material volume per length unit influence on height parameter

This is the strongest relation found for track height. Traverse and wire feed speeds are the two process parameters that affect this rate.

5.2.2.2 Width

Figure 5-16 presents measured width values. Tracks present a relatively constant shape variation. They tend to start thin and smoothly grow wider, until they

stabilize. This trend also results from molten pool enlargement due to temperature. Figure 5-17 illustrates how width develops with temperature increase.

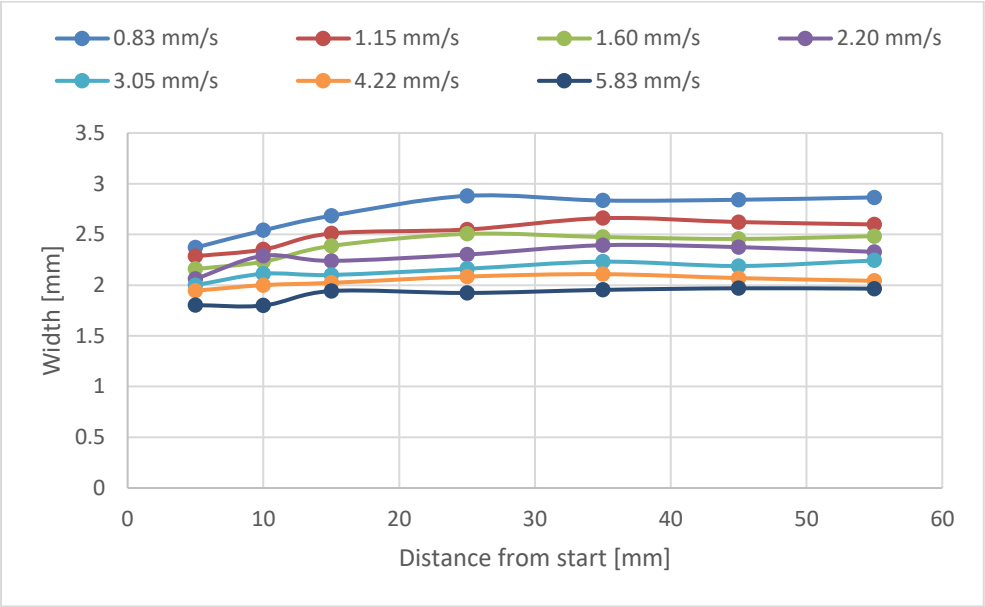

Figure 5-16: Width values measured for traverse speed variation tracks.

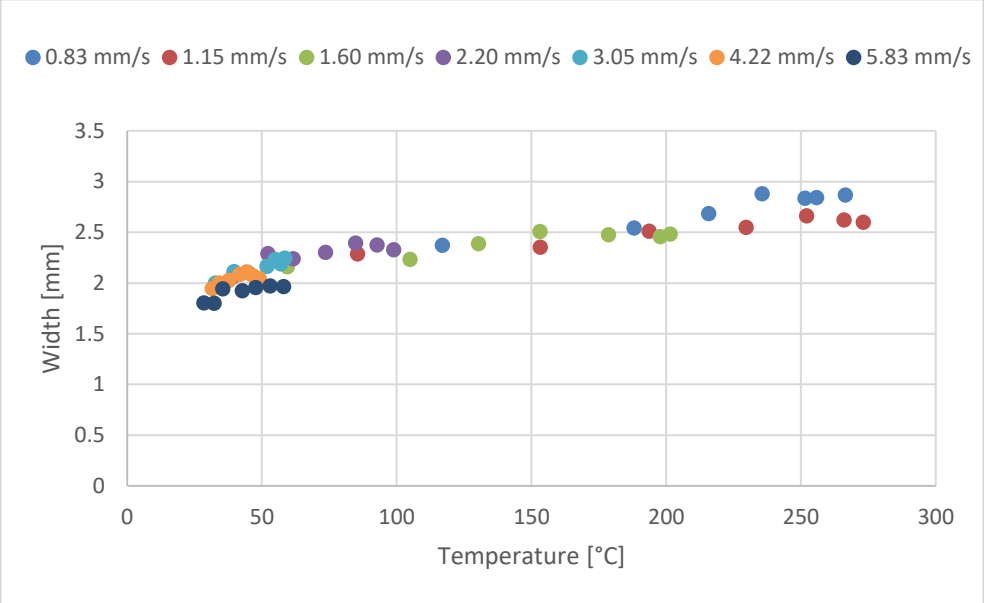

Figure 5-17: Width values of all cross sections and their relation with their respective temperatures

The offset present on Figure 5-13 for height disappears on Figure 5-17, showing how smaller the influence of traverse speed on width is. For the same 700% increase in speed, track final width only decreases 31.7%. Figure 5-18 shows how width varies with traverse speed.

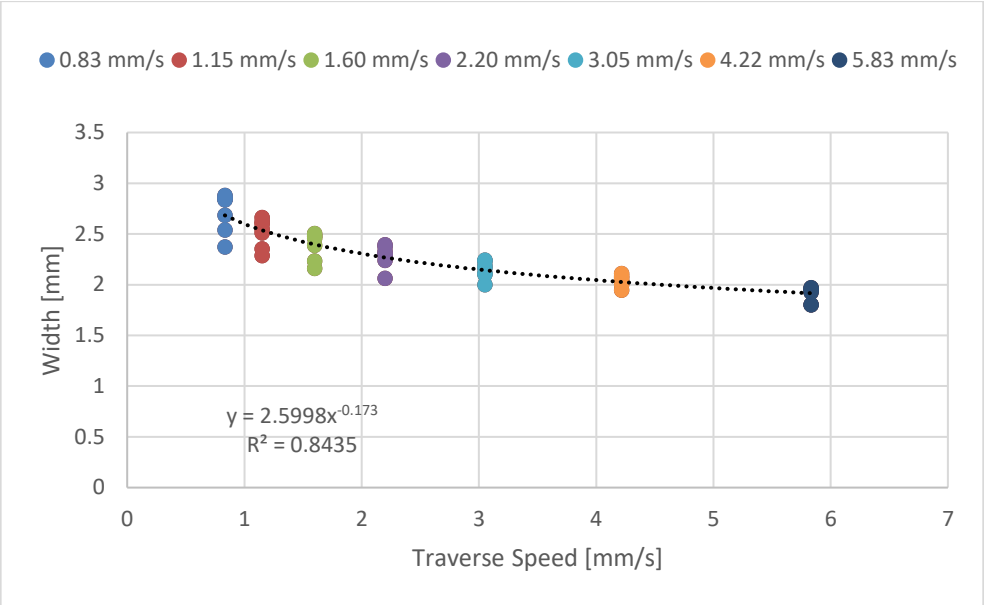

Figure 5-18: Width variation for different traverse speed values.

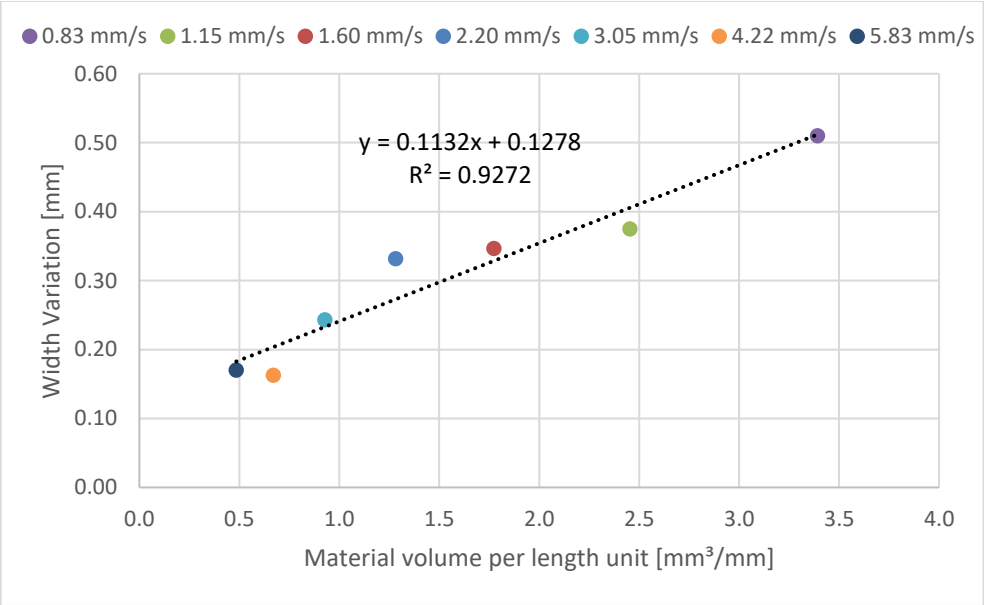

Figure 5-19: Difference of highest and lowest width measurements of each track influenced by the material volume per length unit rate.

The overall influence of traverse speed does not considerably change the width. Width variations along each track, however, do increase with slower speeds. The fastest track has a variation bigger than expected because of the wire mistake on its beginning – seen on Figure 5-9. Figure 5-19 shows the relation between width variation and material volume added per length unit.

5.2.2.3 Track area

As discussed before, tracks tend to be flatter and wider by their ends due to temperature increase during the process. Their area sizes, however, are not affected. As the same volume of material per second is added along the track, cross section areas change their shapes, but not their sizes. Figure 5-20 shows area measurements along each track. It also shows each track average (full lines) and expected (dashed lines) areas. The expected, theoretical area of a track is calculated based on wire dimension and process parameters. It is calculated accordingly to *(5)*.

$$A_E[mm^2] = \frac{\pi * {D_W}^2[mm^2]}{4} * \frac{S_W\left[\frac{mm}{s}\right]}{S\left[\frac{mm}{s}\right]} \quad (5)$$

Where A_E stands for expected area, D_W stands for wire diameter, S_W stands for wire feed speed and S stands for traverse speed.

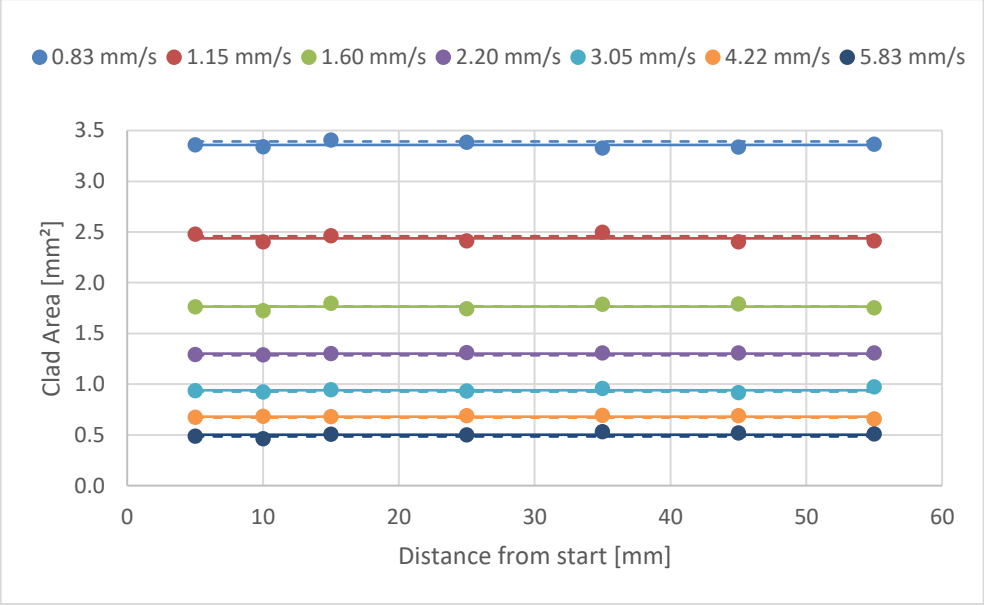

Figure 5-20: Clad area for different traverse speeds. Dots represent measured data. Full lines represent the average of each clad's area measurements, while dashed lines represent each clad expected area.

Only very small variations occur along the tracks due to natural random factors and measurement errors. An increase on track dilution can also interfere on the area variation, but its effect is not noticeable. On the slowest track, measured areas diverged less than 2.0% of the theoretical value. The fastest track presents the highest variation: 9.5%. An increase on this variation is expected for faster traverse speeds,

as the process becomes less stable. On Figure 5-21, it is possible to notice how traverse speed influences on measured area variations.

Track area is strongly related to the material volume input per length unit. If *(5)* is not measured in [mm²], but in [mm³/mm], it represents the material volume input per length unit. Figure 5-22 shows the strong, linear relation of this factor and track's area.

As wire feed speed is constant for all tracks, a direct, strong relation between track area and traverse speed exists. This relation can be seen on Figure 5-23.

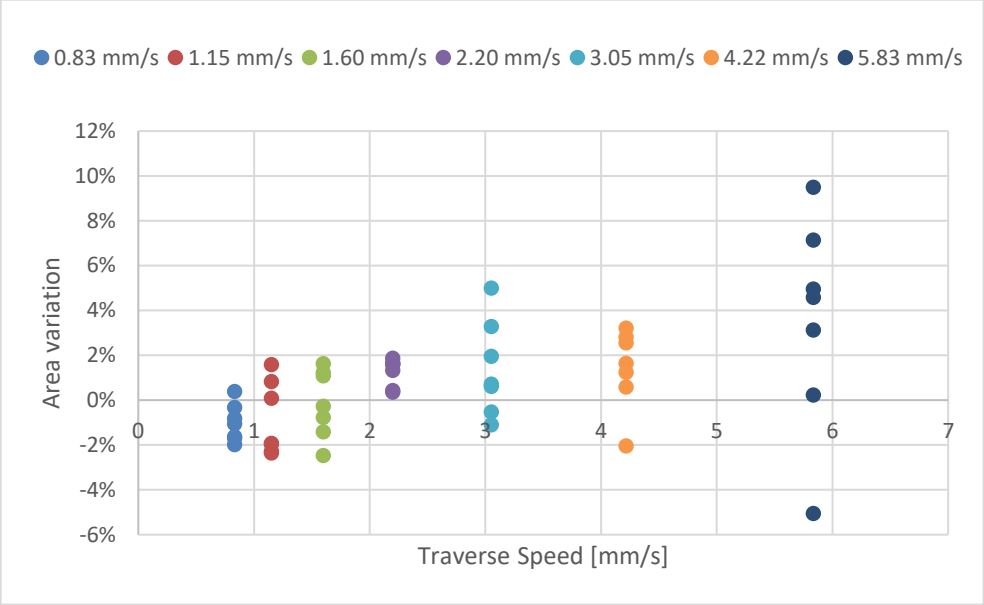

Figure 5-21: Area variation and traverse speed relation. Area variation is a measurement of how bigger or smaller the measured area is proportional to the theoretical area.

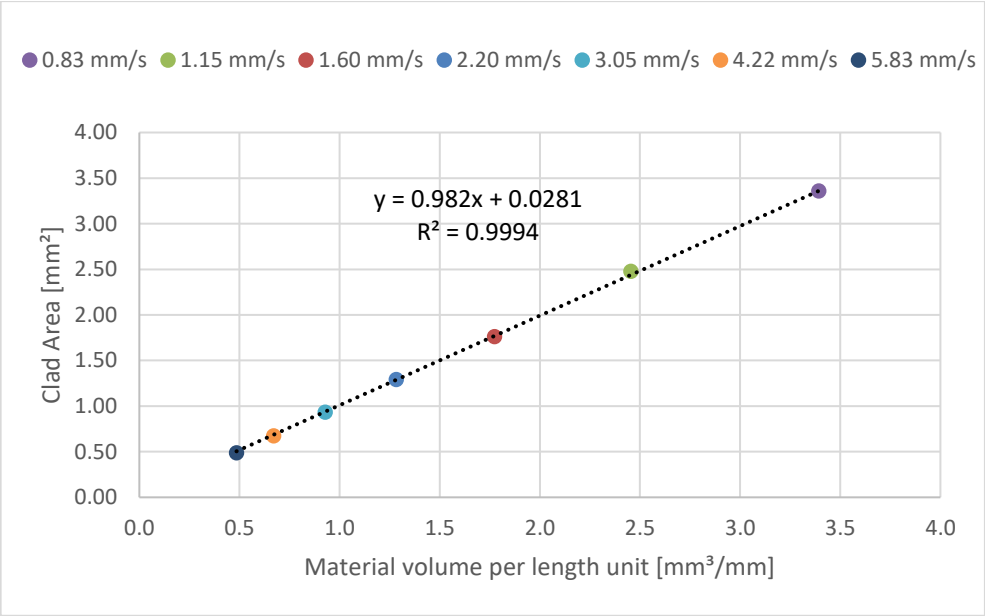

Figure 5-22: Relation of track area and material volume input per length rate.

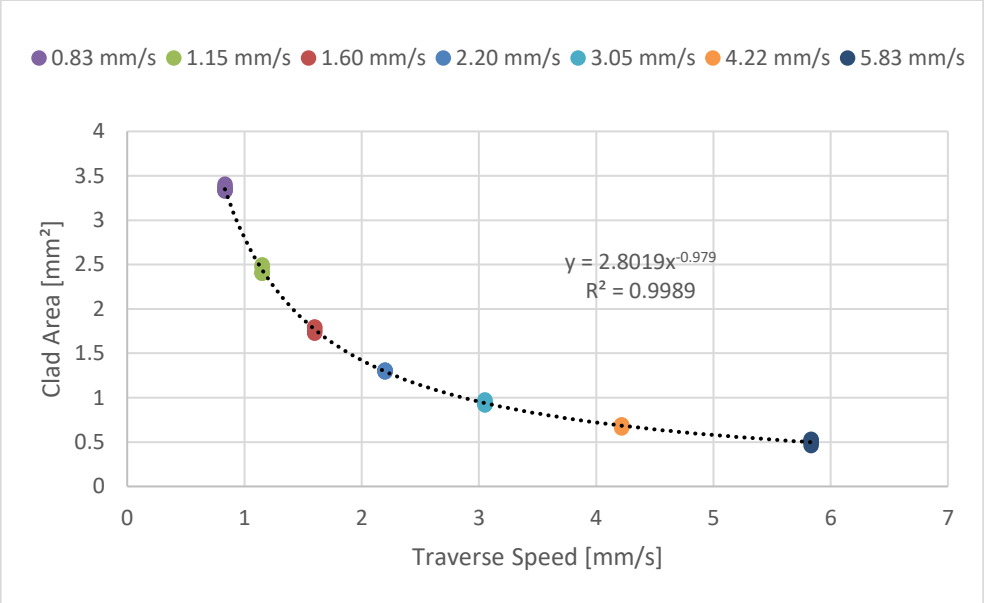

Figure 5-23: Track area and traverse speed relation.

5.2.3 Laser power influence on temperature

On tracks 8 to 13, traverse speed is 2.20 mm/s, while laser power varies from 572 W to 968 W, as described on section 4.1. Temperature recorded is from the same region as on the traverse speed case, as described on section 3.2.4. Recorded data for those tracks are on Figure 5-24.

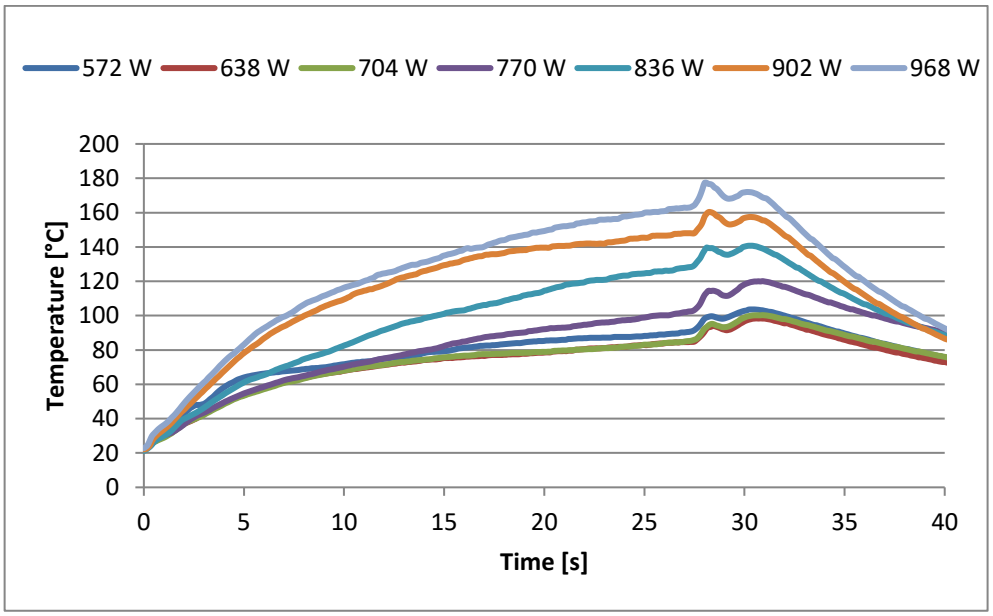

Figure 5-24: Temperature record for tracks with constant traverse speed and different laser powers.

Figure 5-25 shows that temperature increases with laser power, as expected. The track cladded with the lowest power, however, is unexpectedly hotter. The track's surface explains this behavior (Figure 5-25). On its beginning (left side), a small region was affected by the laser but without visible wire cladding. It happened because there was not enough energy to melt the wire while the laser focused that region. Without the material volume input, less heat dissipates from the substrate, explaining its bigger initial heating. As soon as the wire reaches fusion temperature and melts, all the wire volume fed until this moment bonds to the substrate at once. Due to surface tensions, it assumes a globular shape. This sphere's surface tensions disturb track geometry on the next millimeters, generating visible geometrical and temperature oscillations. Those oscillations vanish on the first 15 mm of the track. This effect is also present on tracks cladded with 638 W and 704 W of laser power, but attenuated.

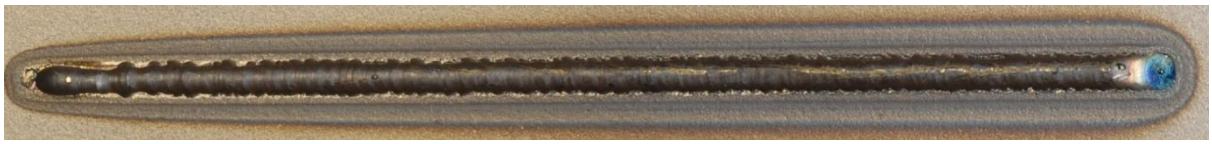

Figure 5-25: Surface of the track cladded with 572 W laser power. Too low laser power generated a large geometry variation on its beginning (left side).

The wire misplacement problem with the fastest track of section 5.2.1 also generates a similar overheating. By track surface, however, it is possible to see that different problems occurred.

Temperature values on cross section regions were acquired identically as explained on section 5.2.1. Values obtained are on Figure 5-26.

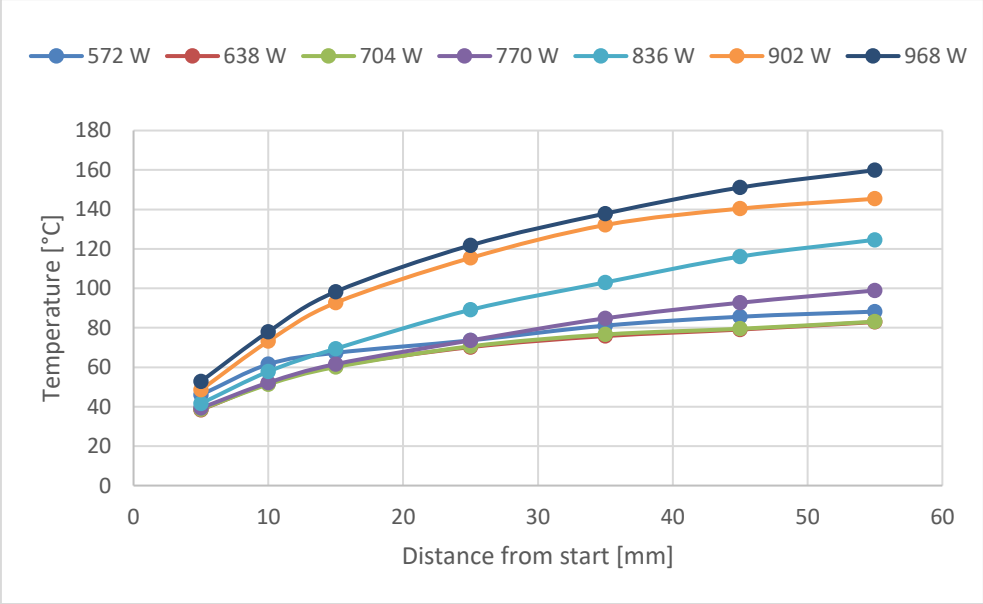

Figure 5-26: Temperature values for each cross section region of power variation tracks.

To analyze laser power influence on temperature, the data was reorganized as shown on Figure 5-27. From the graph, it is noticeable how track temperature increases with laser power. It is also noticeable how the explained disturbance affected the temperature of the track cladded with 572 W.

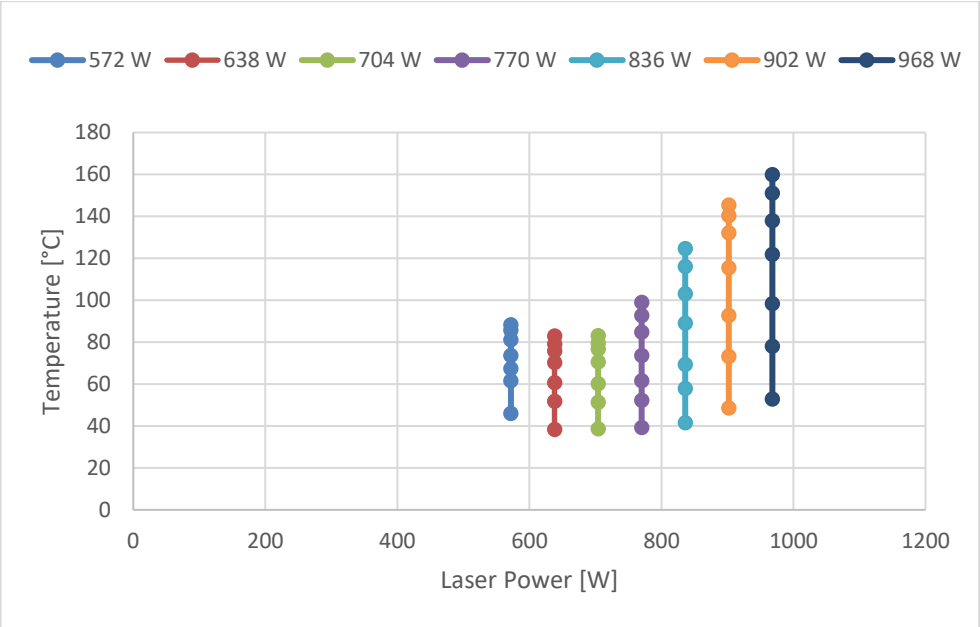

Figure 5-27: Laser power influence on track temperature

Each track's temperature value increases with laser power due to the increase of energy per length unit. As calculated in *(5)*, the total energy absorbed on each track's first 5 mm is on *(6)*. Results for those track parameters are on Table 5-3.

$$E[J] = \frac{d[mm] * P\left[\frac{J}{s}\right]}{S\left[\frac{mm}{s}\right]} = \frac{5[mm] * P\left[\frac{J}{s}\right]}{2.20\left[\frac{mm}{s}\right]} \quad (6)$$

Table 5-3: Energy emitted from the laser source on the first 5 mm of each track.

Laser power [W]	572	638	704	770	836	902	968
Energy $[J]$	1300	1450	1600	1750	1900	2050	2200

Higher laser power results in more absorbed energy, furthermore, higher temperatures. The relation of temperature and laser's total emitted energy is on Figure 5-28.

The results shown in Figure 5-24 and Figure 5-28 permit to affirm that track temperature would stabilize after reaching a certain level, even if those functions are modelled as logarithm functions. When energy input is equal to energy loses, temperature stops to increase. This level is achievable as energy loses also increase with temperature.

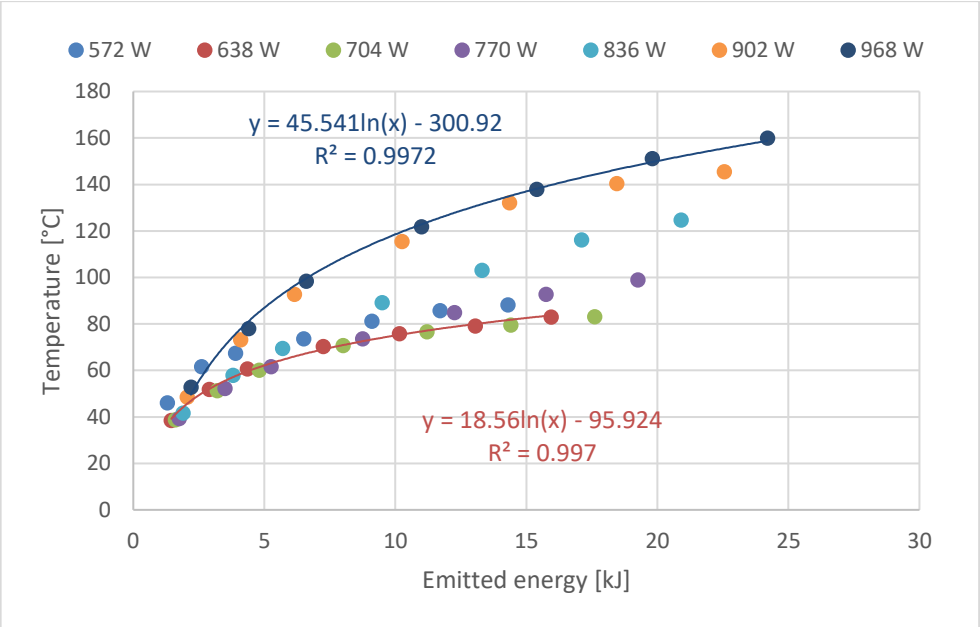

Figure 5-28: Temperature behavior as the laser emits more energy. Parameters are strongly correlated ($R^2 > 0.99$).

5.2.4 Laser power influence on track geometry

As on the previous case, track geometries were obtained from cross section images accordingly to the procedure described on section 4.5. Each geometric dimension is analyzed, and its relations with laser power and other parameters, discussed.

5.2.4.1 Height

The relations of measured height values and position for each track are shown on Figure 5-29. A graph relating track height and time is not necessary, as all tracks were cladded at the same speed.

During process a molten pool forms on the substrate's surface and the wire enters the laser beam at solid phase. After absorbing an amount of energy, it melts and is incorporated to the molten pool. A stronger laser beam heats the molten pool more, enlarging it and reducing its viscosity. The molten metal flows over the substrate accordingly to its viscosity. Height is than decreased by a bigger metal flow. This height decrease influenced by laser power is on Figure 5-30. Figure 5-31 shows how height varies accordingly to temperature.

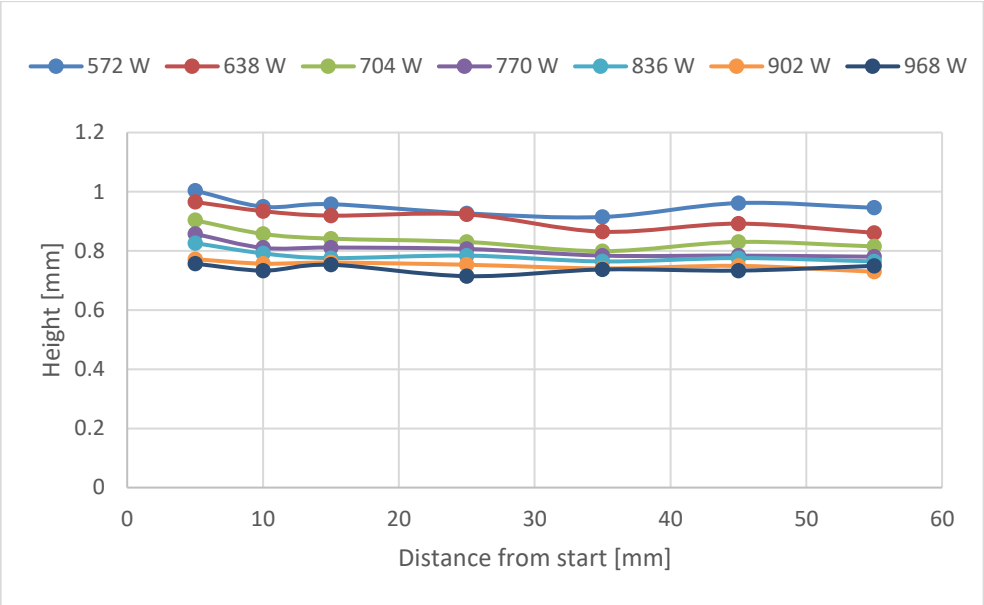

Figure 5-29: Height values for tracks with different laser powers.

Tracks cladded with higher laser powers have a narrower range of heights. Higher laser powers allow the molten pool to reach higher temperatures. On higher temperatures, viscosity changes are smaller. Therefore, measured height values vary less. On Figure 5-31, temperature on the first cross section of the two tracks with highest laser power values already achieved this level; therefore, those are the tracks with the smaller variations. This is also visible in Figure 5-29, where the height variation between the first and the second cross sections is the smallest for those two tracks.

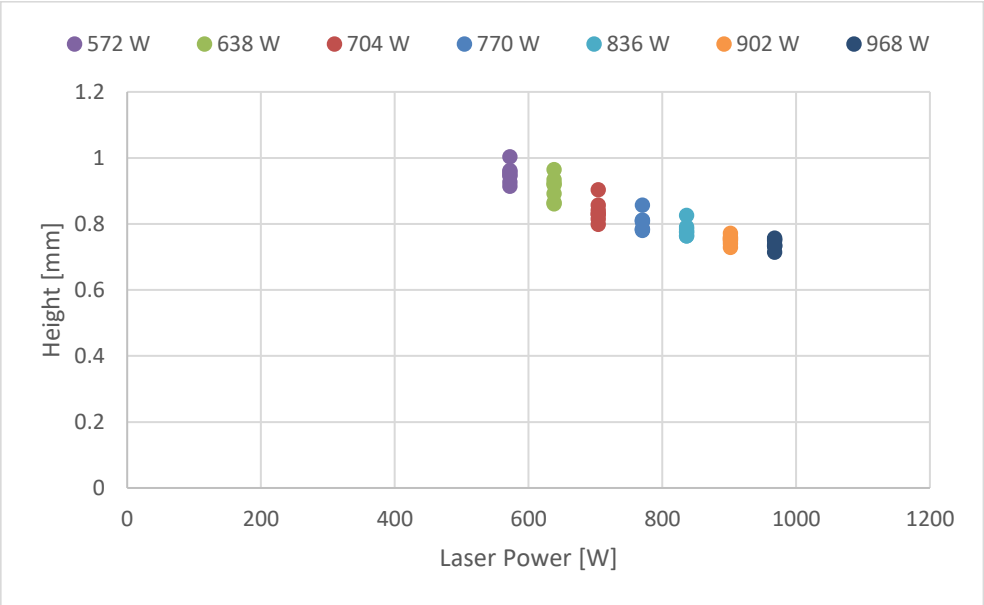

Figure 5-30: Height values and their relation with laser power. As tracks absorb more energy from a higher power laser, they become flatter.

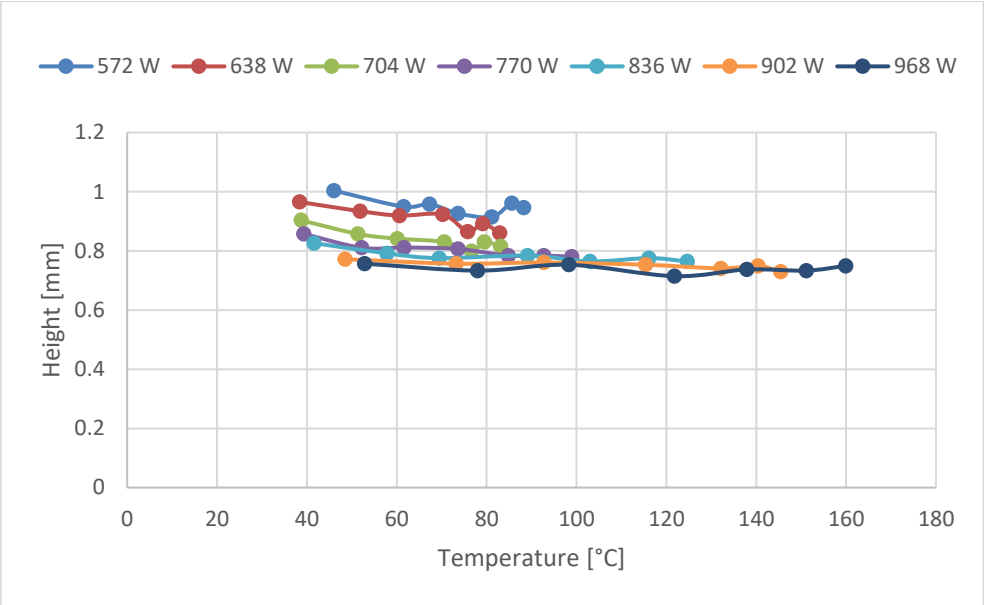

Figure 5-31: Height values related to temperature along tracks.

5.2.4.2 Width

As already explained, tracks tend to become wider with higher temperatures generated by higher laser beam powers. Results obtained on Figure 5-32 confirm this fact.

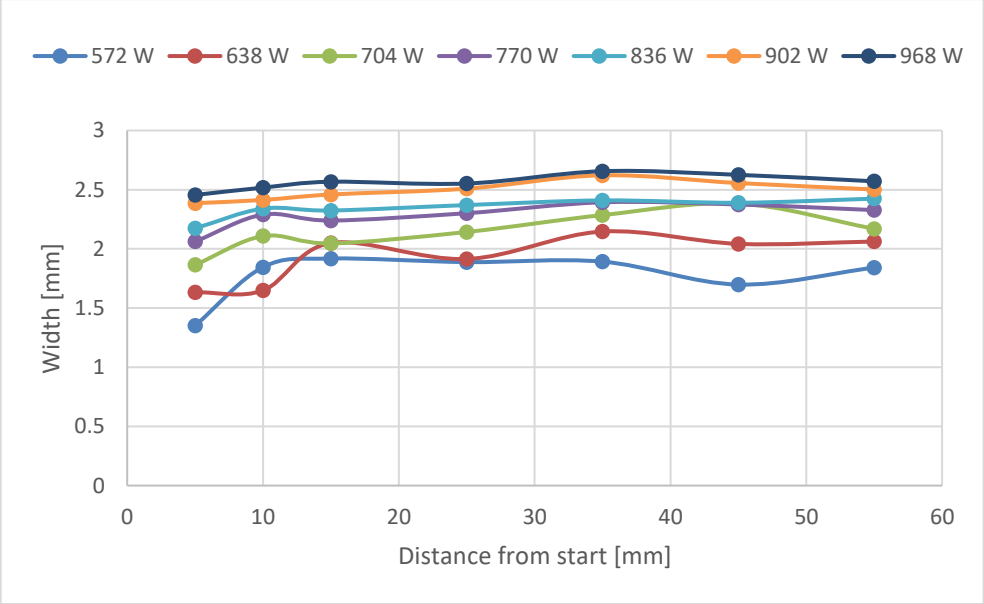

Figure 5-32: Width values measured for laser power varied tracks.

Track width increases with laser power until a certain limit, which is determined by laser beam's spot width. On the current setup, however, a scanner device deflects the beam along a line perpendicular to cladding direction. The amplitude of this line has the strongest influence on this dimension. On these experiments, however, this parameter remains constant.

Besides the viscosity variation effect, the laser power has another influence on track width. When the power rises, the energy density profile of the laser beam also changes. The size of the region with enough energy density for melting the wire grows when increasing laser power, leading to wider tracks. Both effects are present on Figure 5-33.

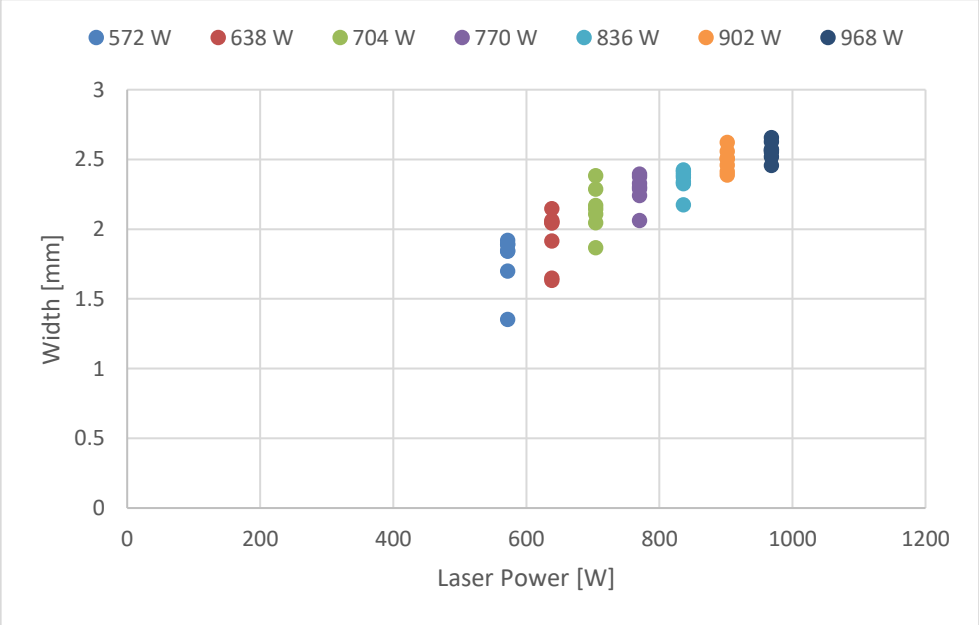

Figure 5-33: Laser power influence on width measurements.

From this graph, it is also visible how higher laser powers result in more stable tracks. The three tracks cladded with the lowest laser power present high width variations along them, especially on the first two (smaller) cross sections. The reason for that is the disturbance described in section 5.2.3. Surface of those tracks are on Figure 5-34. Tracks cladded with laser power over 900 W have small variations.

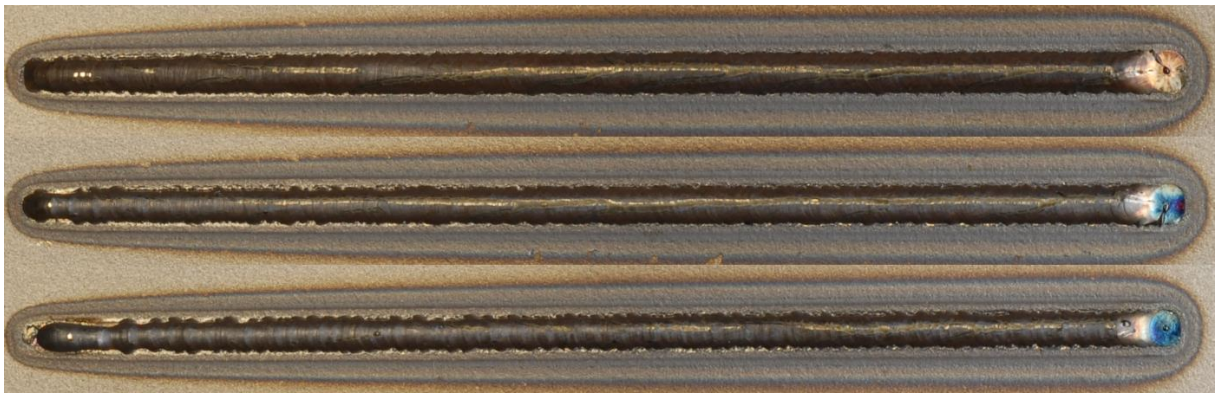

Figure 5-34: Surfaces of the tracks cladded with the same speed with 704 W (on top), 638 W (middle) and 572 W (on bottom). Track disturbance at the beginning increases when lowering laser power.

5.2.4.3 Track area

Track area is a parameter strongly related to the material volume per length unit rate. As this is a constant value for these tracks, no variation is expected. The measurements on Figure 5-35 confirm it.

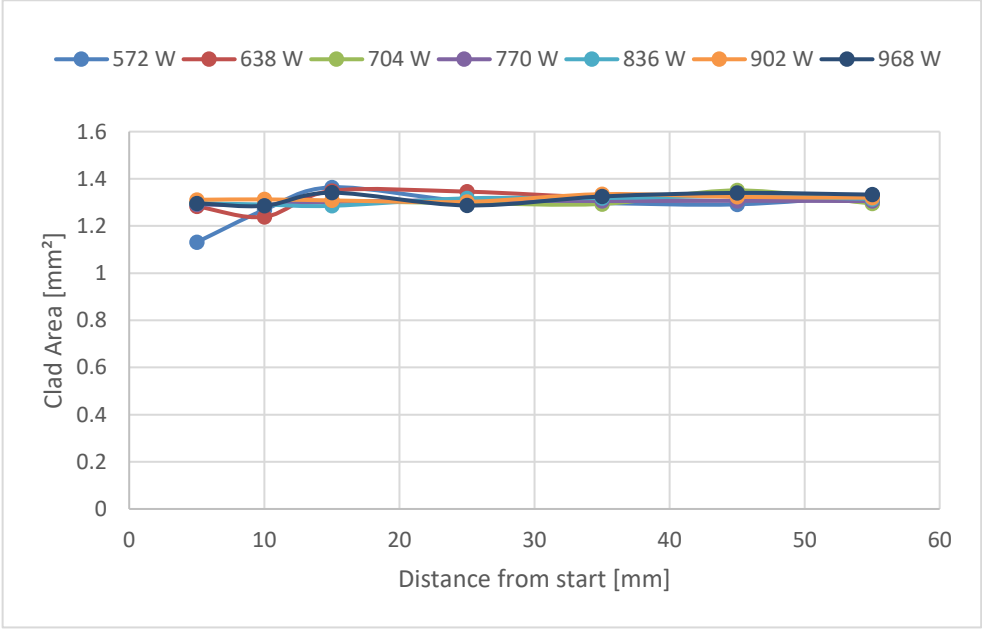

Figure 5-35: Track area values for different laser powers.

Different laser powers lead to different track profiles. Tracks become flatter, wider for high power values and higher, thinner for low ones. Figure 5-36 shows an interesting relation of how are height and width related for different laser powers. Those

dimensions always keep a constant height to width ratio. Outthought there are many variations on cladded area profile, track area size, however, stays the same.

Only one cross section presents an unexpected value. The area from the first cross section of the track cladded by 572 W is smaller than it should. Figure 5-37 shows the huge difference between first and second cross sections of this track. The cited disturbance on its beginning is the reason for that. That unexpected area could have been either smaller or larger than expected, depending on the position from where it was obtained.

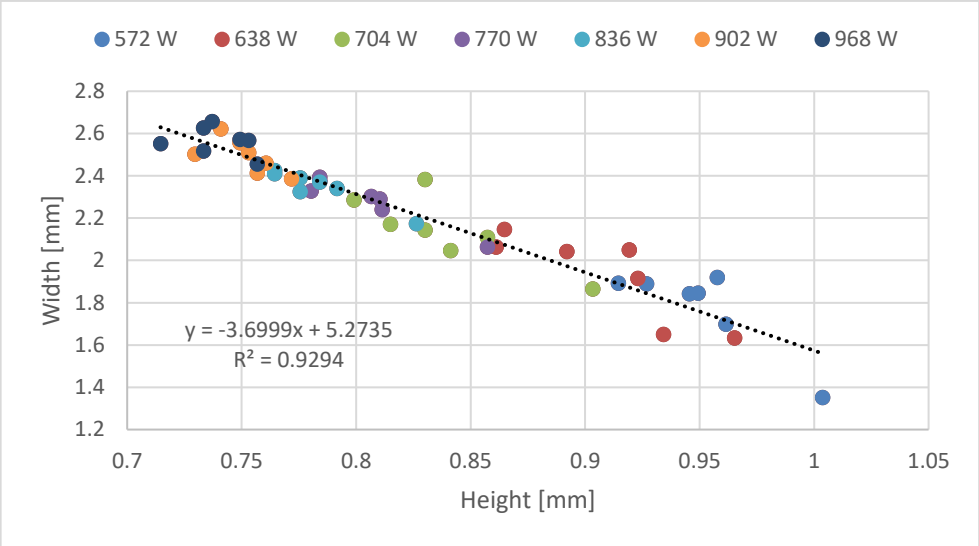

Figure 5-36: Width and height relation for different laser powers.

Figure 5-37: First (left) and second (right) cross section images of the track cladded by 572 W. Eventhought there is only 5 mm between the regions from where those photos where taken, differences on area shapes and sizes are clear.

When analyzing the graph on Figure 5-38, it is noticeable that track area has higher variations on tracks cladded with lower laser power. Again, the disturbance on

the beginning of tracks with lower laser power explains it. Besides that, no influence of laser power on this parameter exists. Dilution also can influence on the track areas as it raises along the track, but this influence is again not noticeable, once there is no trend on the tracks area variation.

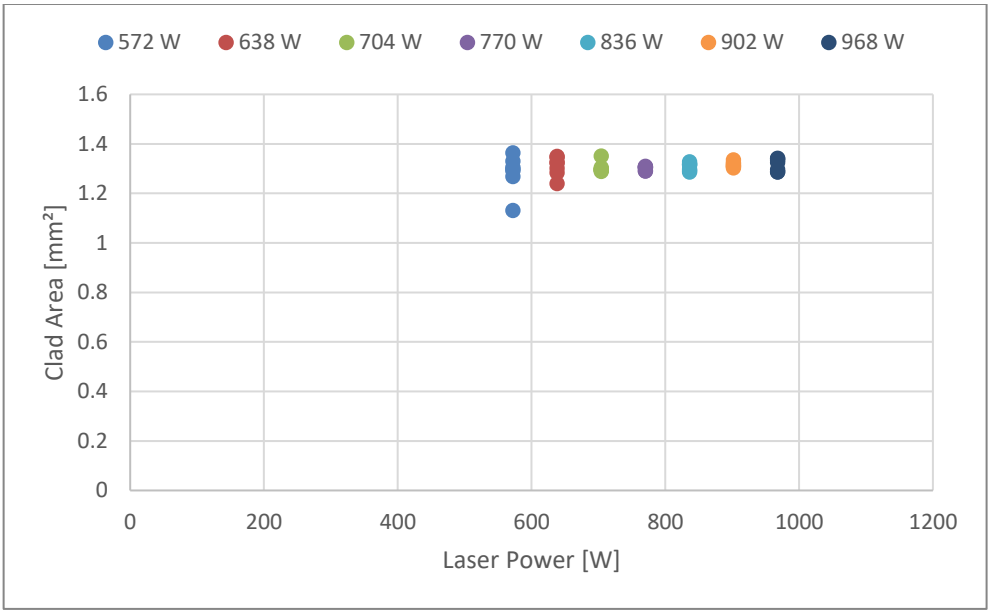

Figure 5-38: Track area and laser power relation.

5.2.5 Energy per length unit and track geometry

The next step after analyzing the effect of each individual parameter on track geometry is to analyze them together. To quantify those relations, the energy per length unit rate is used. This parameter is important for allowing comparability of all tracks. Its calculation is on *(7)*.

$$E\left[\frac{J}{mm}\right] = \frac{P}{S}\left[\frac{\frac{J}{s}}{\frac{mm}{s}}\right] \tag{7}$$

Even when analyzing both influences together, it is still possible to identify two different trends corresponding to each parameter variation, visible on Figure 5-39, Figure 5-40 and Figure 5-41. The trend with the bigger energy range corresponds to the tracks with constant laser power, while the tracks on the smaller trend have constant traverse speed.

On Figure 5-39, height values increase with slower traverse speeds – increasing the amount of energy per length unit. However, height decreases when the laser power

is reduced – decreasing the amount of energy per length unit. Thus, height presents two controversial behaviors when increasing the energy input.

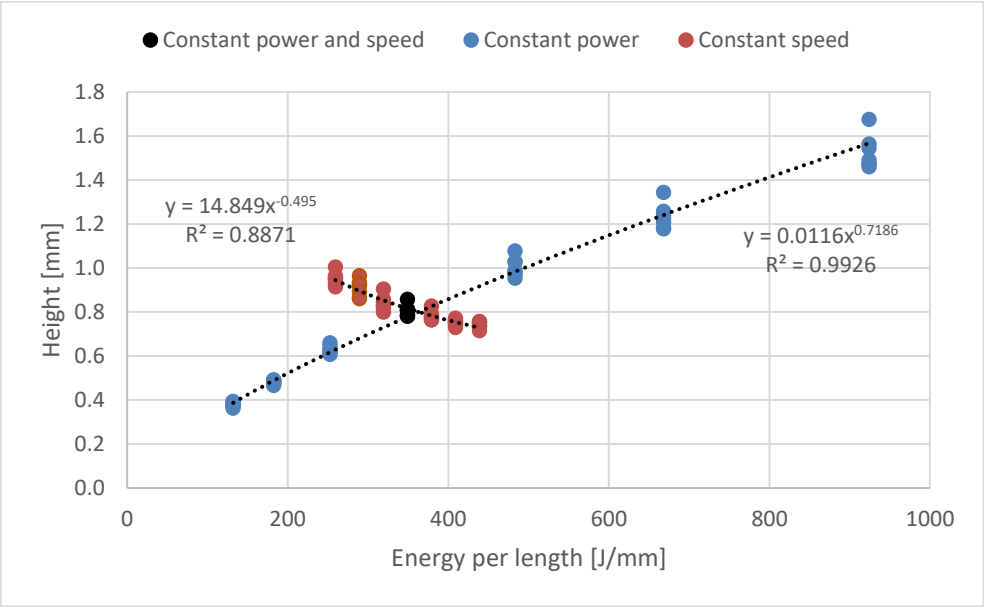

Figure 5-39: Height values of all tracks and their relation with the energy per length unit rate.

Both trends for width values increase with energy. On the longest trend, reducing traverse speed increases the material volume per length unit rate, leading to bigger, wider track areas. On the shortest trend, higher laser powers lowers molten pool's viscosity, also generating wider tracks.

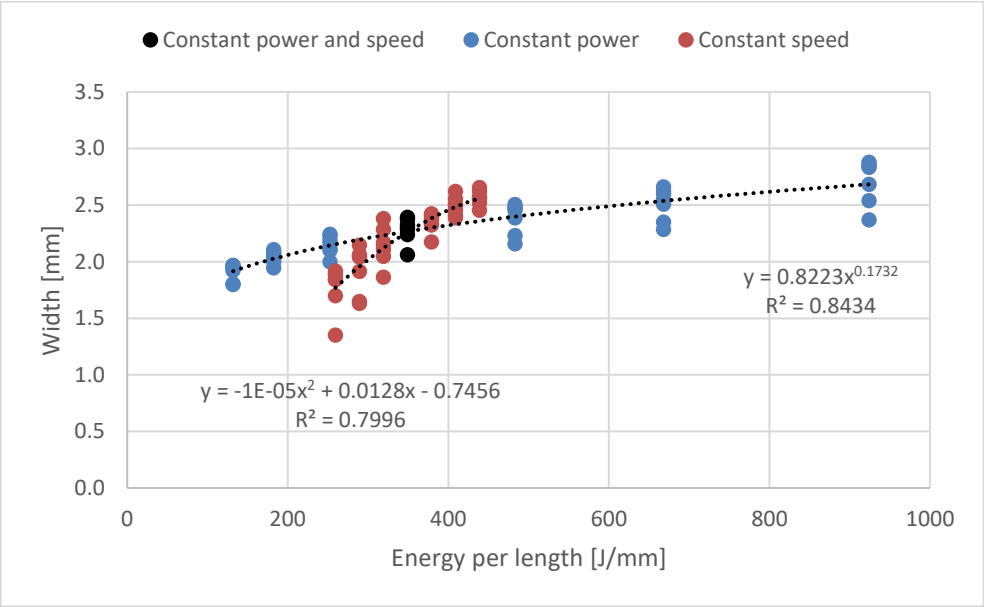

Figure 5-40: Width values of all tracks and their relation with energy per length unit.

Only traverse speed affects track area values. The material volume per length unit rate increases with slower speeds, enlarging track areas. Laser power, however, only changes track area profile, but not its size.

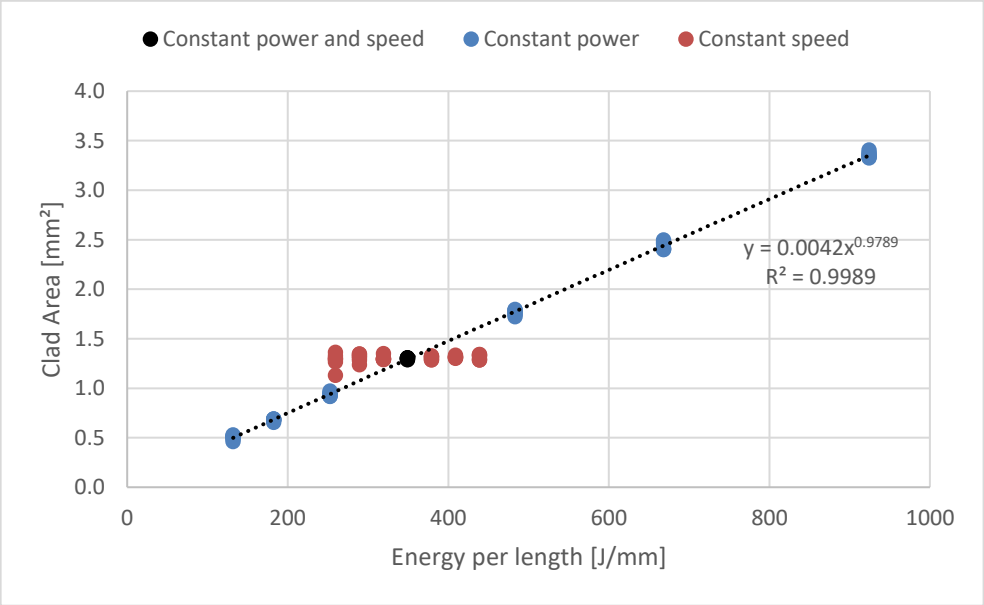

Figure 5-41: Track area values of all tracks and their relation with energy per length unit.

Chapter 6 Modeling

From the results obtained, information about the process behavior is now available. The influence of traverse speed and laser power on height, width and area of the tracks is clearer. Many trends on geometry variation appeared when varying those process parameters. With this acquired knowledge, the next step is to propose models to predict each of the studied dimensions based on those process parameters.

On this chapter, this modeling is proposed. It is based on the thirteen tracks performed. After that, the purposed model is validated predicting the geometry of four more tracks, those cladded with a combination of maximum and minimum traverse speeds and laser powers (tracks 14-17 of Table 4-1 at page 24).

The first dimension predicted is the track area, once its size is not altered by laser power. Later, a ratio between height and width of each track is predicted. This ratio is necessary to enhance comparability between tracks. The added material per length unit rate varies for different traverse speeds, what does interfere considerably on final track height and width. Dividing height per width reduces the influence of this factor, improving the quality of the prediction. Finally, the dimensions of track height and width are predicted approximating track shape to geometrical features.

6.1 Track area prediction

The easiest dimension to model is track area. It depends directly on the material volume per length unit rate, which – with constant wire feed speed – depends only on traverse speed. Calculation of this rate is in *(4)* on page 39. Figure 5-22 on page 44 already shows the linear relation between track area and that rate. Figure 6-1 below shows again this relation, as well as the trends for maximum and minimum area values based on their volume input per length unit rate. Based on these trends, it is possible to predict the areas for the tracks with the combination of maximum and minimum traverse speeds and laser powers. Table 6-1 shows the results obtained from these trends, calculated as shown in (8).

$$0.99021034 * \mathrm{V} + 0.05963906 \geq \mathrm{A}(V) \geq 0.97985155 * \mathrm{V} + 0.00026010 \quad (8)$$

Table 6-1: Maximum and minimum expected areas for the four tracks. Tracks are sorted by energy per length unit level

Energy per length unit [J/mm]	Laser Power [W]	Traverse Speed [mm/s]	Volume Input [mm³/mm]	Expected Maximum Area [mm²]	Expected Minimum Area [mm²]
98.1	572	5.83	0.48	0.54	0.47
166.0	968	5.83	0.48	0.54	0.47
686.7	572	0.83	3.40	3.42	3.32
1162.1	968	0.83	3.40	3.42	3.32

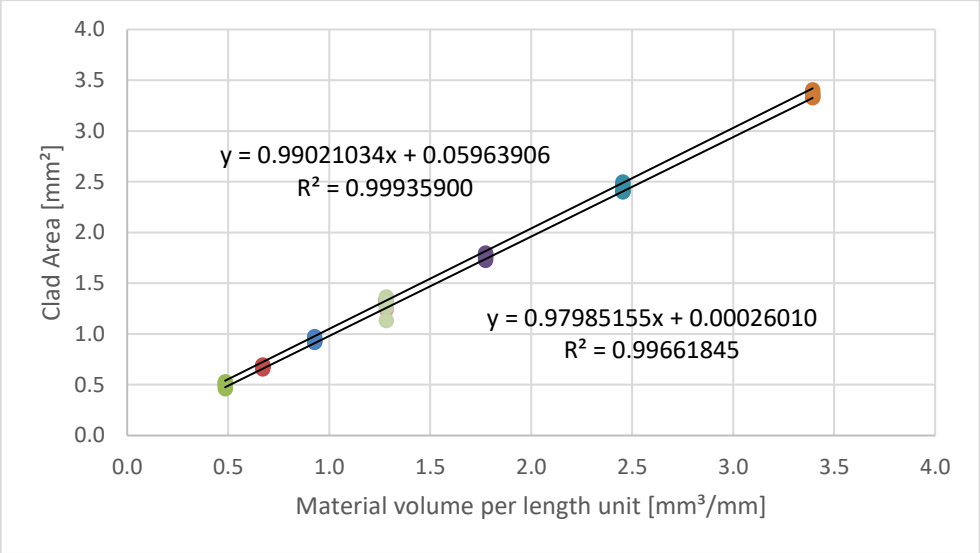

Figure 6-1: Maximum and minimum track areas for different material volume input rates.

After measuring the tracks cladded with the parameters on Table 6-1, the results are compared on Table 6-2. The largest discrepancy appears on the track cladded with the highest traverse speed and the lowest laser power, where the predicted minimum area is 135% bigger than the real measured. When looking at this track's surface (Figure 6-2), the reason for that becomes obvious: it is not a stable track. The energy per length unit of this track is of 98.1 J/mm, which is not enough to melt the wire properly. The result is a track with instable geometry, lack of wire fusion and lack of metallic bond, with no commercial use.

Figure 6-2: Surface of the track cladded with maximum traverse speed and minimum laser power. The energy per length unit is not high enough to melt the wire properly.

Table 6-2: Real areas measured for the tracks with maximum and minimum parameters values.

Laser Power [W]	Traverse Speed [mm/s]	Energy per length unit [J/mm]	Max Predicted Area [mm²]	Max Real Area [mm²]	Max Area Error [%]	Min Predicted Area [mm²]	Min Real Area [mm²]	Min Area Error [%]
572	5.83	98.1	0.54	0.59	-8.47%	0.47	0.2	135%
968	5.83	166.0	0.54	0.52	3.85%	0.47	0.47	0%
572	0.83	686.7	3.42	3.57	-4.20%	3.32	3.24	2.47%
968	0.83	1162.1	3.42	3.41	0.29%	3.32	3.3	0.61%

The most accurate prediction is for the track cladded with maximum laser power and minimum traverse speed, resulting on the highest energy per length unit rate of all tracks. This fact leads do the question if the accuracy of this model can be estimated based on the energy per length rate. The tracks with intermediate energy levels show that this is not true, as no particular trend is found. What is visible is the increase on prediction accuracy on the tracks with the high laser power level, which are also the tracks with the most stable geometry, as seen on Figure 6-3.

The modeling proposed seems to predict well the area of the tracks with constant geometry. More geometrical stability, however, links to higher laser power. This behavior was already noticed on Figure 5-38, where the oscillation of area values is higher for lower laser powers. With the exception of the track with the lowest energy per length input rate, all predictions resulted in errors below 5%.

Figure 6-3: Tracks cladded with the maximum and minimum parameters values. Tracks are sorted by energy per length unit rate, from lowest (top track) to highest (bottom track).

6.2 Height to width ratio prediction

As observed on section 5.2.5, both height and width values present different trends whenever varying traverse speed or laser power. The graphs in Figure 5-39 and Figure 5-40 show those trends. To improve comparability, the ratio between height and width is predicted instead. The relation between this ratio and the energy per length unit rate is on Figure 6-4. The trends are for the maximum and the minimum expected height to width ratio values, all of them having the shape of power functions.

Even when analyzing this ratio, the two trends corresponding to each process parameter are still present. It means that laser power and traverse speed influence the track geometry in a way that cannot be quantified by the energy per length rate. Therefore, height to width ratio is not calculated as a function of energy, but of both laser power and traverse speed.

An approach considering the influences of laser power and traverse speed as independents is taken. The main reason for that is the lack of data to analyze both influences together. A linear, independent model perfectly relating the process parameters to this ratio is not expected. Thus, this approach is a simplified, easier solution to predict the ratio based on those process parameters.

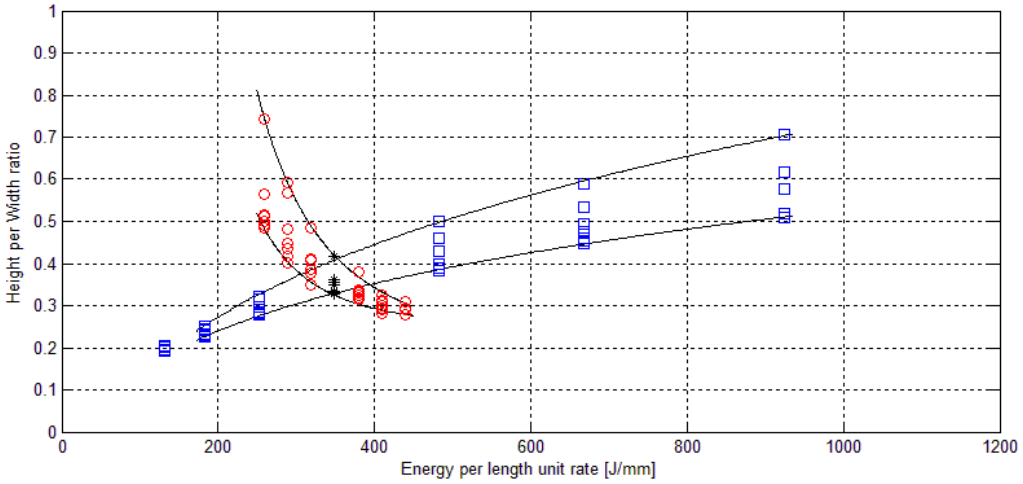

Figure 6-4: Relation between height per width ratio and energy per length unit. Red circles represent the ratio for tracks which have constant traverse speed, while blue squares, constant laser power.The track with the lowest energy is not considered on this calculation as it had a wire missalignment problem on its beginning.

The relations between the ratio and the process parameters have the shapes quantified in (9). The form (10) groups the influences of both parameters based on the superposition principle, assuming linearity between them.

$$\frac{h}{w}(P, S_{const}) = \alpha * P^{\beta} + \gamma \qquad \frac{h}{w}(P_{const}, S) = \alpha * S^{\beta} + \gamma \tag{9}$$

$$\frac{h}{w}(P, S) = \alpha_P * P^{\beta_P} + \alpha_S * S^{\beta_S} \tag{10}$$

The data was fitted into two equations with the shape of (10), one for the maximum predicted values of the height to width ratios, the other for the minimum ones. The curve fitting tool of the software Matlab from MathWorks® was used for the fitting. Formulas obtained are *(11)* and *(12)*. Surfaces generated are on Figure 6-5.

$$\frac{h}{w_{MAX}} = (5.57 * 10^{7}) * P^{-2.917} + 0.428 * S^{-1.012} \tag{11}$$

$$\frac{h}{w_{MIN}} = (3.57 * 10^{6}) * P^{-2.589} + 0.357 * S^{-0.7147} \tag{12}$$

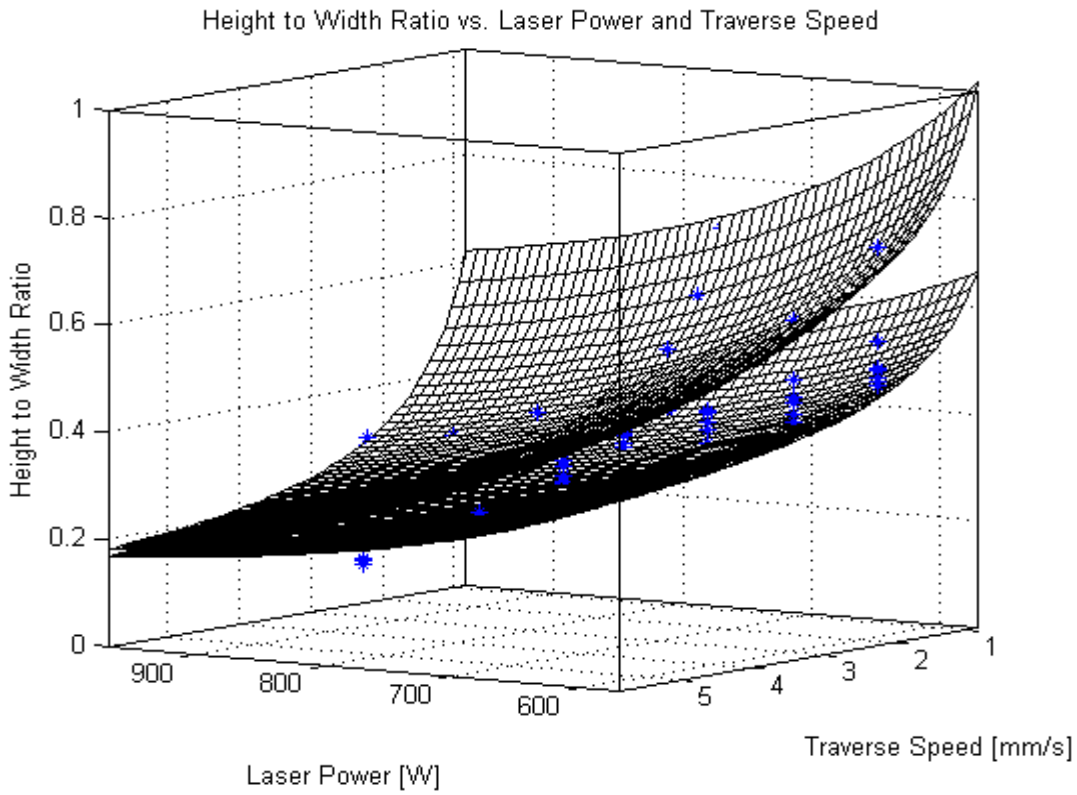

Figure 6-5: Surfaces modeled for maximum and minimum values of height to width ratio. Blue dots correspond to the ratio values for each cross section of the tracks.

Table 6-3 shows the real and predicted values for the tracks on Figure 6-4. Errors beneath 5% are predominant, once the surfaces were fitted based on this data. Larger errors appear on tracks with traverse speed of 4.22 mm/s and 5.83 mm/s, showing that this model does not work properly for faster traverse speeds. Track with traverse speed of 5.83 mm/s also has a bigger error because of its already cited wire misplacement problem.

After obtaining equations (11) and (12), the ratios for the tracks with maximum and minimum process parameters values are calculated and compared to real measured values. Results are on Table 6-4. Measured values are plotted with the surfaces on Figure 6-6.

The predicted ratio values have errors below 10% for the two tracks with the slowest speed. The error of 132.13%, however, results from the surface of this respective track. As already seen in Figure 6-2, it is highly irregular, resulting in unpredictable geometry. On the remaining track – with both highest traverse speed and laser power – the minimum predicted ratio has a relatively higher error, which

confirms the non-reliability of this model for higher traverse speeds, as mentioned on Table 6-3.

Table 6-3: Real and predicted height to width ratio values.

Power [W]	Speed [mm/s]	Real Max HW Ratio	Predicted Max HW Ratio	Max HW Ratio Error [%]	Real Min HW Ratio	Predicted Min HW Ratio	Min HW Ratio Error [%]
770	0.83	0.7068	0.7269	2.84	0.5093	0.5264	3.36
770	1.153	0.5879	0.5829	-0.85	0.4491	0.4423	-1.51
770	1.594	0.4989	0.4792	-3.95	0.3843	0.3755	-2.29
770	2.20	0.4158	0.4045	-2.72	0.3276	0.3226	-1.53
770	3.05	0.3225	0.3507	8.74	0.2769	0.2806	1.34
770	4.22	0.2519	0.3120	23.86	0.2254	0.2474	9.76
770	5.83	0.2057	0.2841	38.11	0.1925	0.2210	14.81
572	2.20	0.7429	0.6973	-6.14	0.4834	0.4614	-4.55
638	2.20	0.5911	0.5596	-5.33	0.4029	0.3977	-1.29
704	2.20	0.4844	0.4679	-3.41	0.3484	0.3539	1.58
836	2.20	0.3801	0.3593	-5.47	0.3153	0.2996	-4.98
902	2.20	0.3235	0.3261	0.80	0.2826	0.2824	-0.07
968	2.20	0.3082	0.3012	-2.27	0.2775	0.2691	-3.03

Table 6-4: Predicted values of height to width ratio for the tracks with the maximum and minimum parameters values.

Power [W]	Speed [mm/s]	Energy per length [J/mm]	Real Max HW Ratio	Predict Max HW Ratio	Max HW Ratio Error [%]	Real Min HW Ratio	Predict Min HW Ratio	Min HW Ratio Error [%]
572	5.83	98,1	0.6164	0.5769	-6.41	0.155	0.3598	132.13
968	5.83	166,0	0.1682	0.1807	7.43	0.1439	0.1674	16.33
572	0.83	686,7	0.9325	1.0197	9.35	0.6827	0.6652	-2.56
968	0.83	1162,1	0.5712	0.6236	9.17	0.439	0.4728	7.70

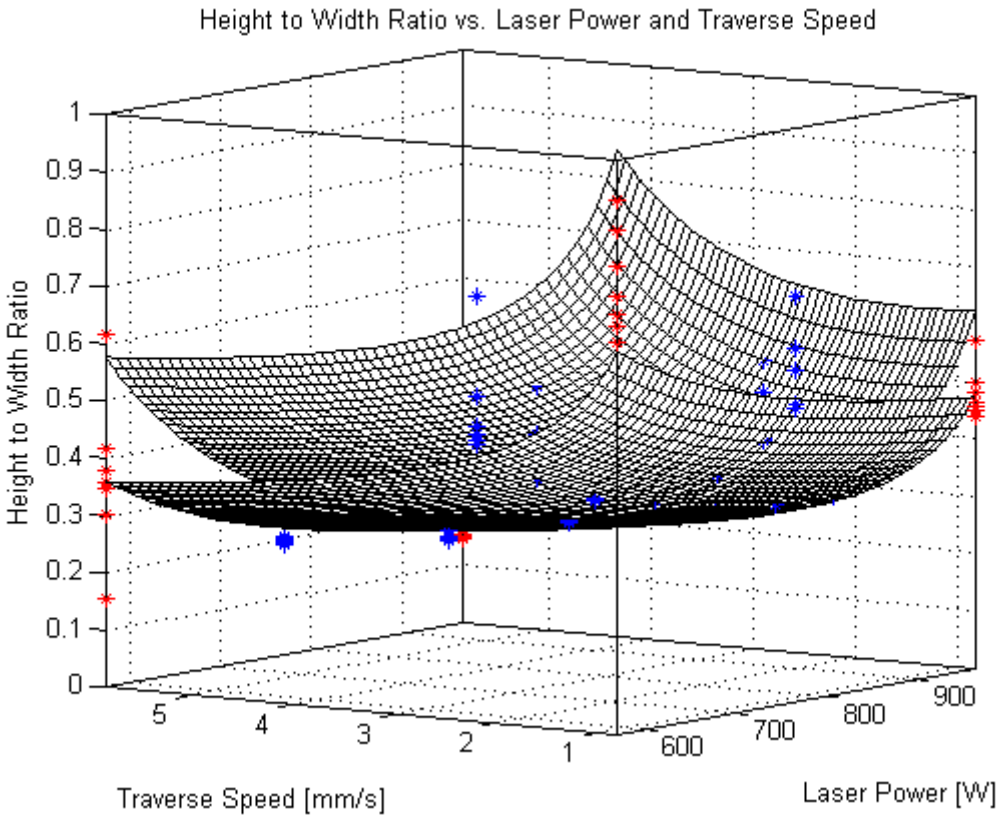

Figure 6-6: Surfaces modeling height to width maximum and minimum expected ratios. Blue dots are the ratios of the cross sections of the first thirteen tracks. Red dots are measured ratios for the tracks with maximum and minimum process parameters values.

Another noticeable fact on the slowest tracks is how higher the error of the maximum ratio is compared to the one of the minimum ratio. The maximum ratio mostly occurs on the beginning of the track, while the minimum, on its end. The reason for that is temperature. The hotter the track is, the flatter, wider it becomes, lowering the height to width ratio. As the thermal gradients on the end of a track are much smaller than on its beginning, it makes the geometry on this region much more stable. Thus, positioning errors when cutting the substrate to obtain cross sections have less influence on the end of the track than on its beginning, leading to smaller errors on the predicted minimum height to width ratio than on the maximum one.

6.3 Height and width prediction

After calculating the predicted values for track area and height to width ratio, it is possible to estimate the values of height and width of each track. To do so, an

assumption about the track shape needs to me made. It is considered to assume one of the three profiles on Figure 6-7. The first two profiles correspond to a section of a circle delimited by a chord. The approximation of the track profile to a circle was already made in laser cladding with powder feeding by Pinkerton in [19] and Cheikh in [18]. The third profile corresponds to a wall geometry, where width reached its maximum – limited by the scanner amplitude.

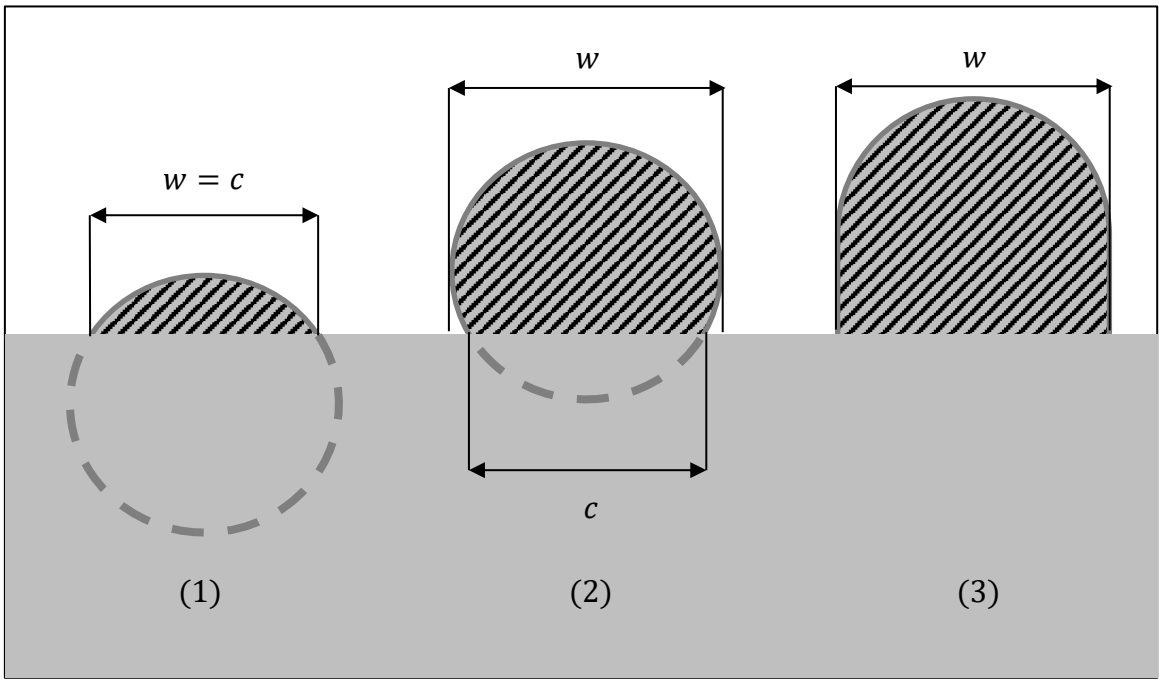

Figure 6-7: Different track area profiles, where w stands for track width; and c, for the chord of the circle.

6.3.1 First case

In both first cases, (13) calculates the area delimited by the chord.

$$A = r^2 * \frac{\theta - \sin\theta}{2} \qquad (13)$$

Where r stands for the circle radius, and θ, for the angle corresponding to the chord, expressed in radians. The first profile corresponds to tracks with height to width ratio equal or below 0.5. In this case, width of the track corresponds to the circle chord.

As shown in (14) and (15), r and θ values can be calculated based on height and width. There, h stands for track height, and w, for track width.

$$r = \frac{h}{2} + \frac{w^2}{8 * h} \tag{14}$$

$$\theta = 2 * \sin^{-1} \frac{w}{2 * r} \tag{15}$$

Height h can be calculated multiplying track width w and height to width ratio γ.

$$h = \gamma * w \tag{16}$$

Replacing *(16)* in *(14)* and *(15)*, r and θ can be calculated as in *(17)* and *(18)*.

$$r = \frac{w}{2} * \frac{\gamma}{\gamma + \frac{1}{4 * \gamma}} \tag{17}$$

$$\theta = 2 * \sin^{-1} \frac{1}{\gamma + \frac{1}{4 * \gamma}} \tag{18}$$

After that, replacing *(17)* and *(18)* on (13) and isolating w, the form for calculating width is obtained, as shown in *(19)*.

$$w = \frac{4 * \gamma}{1 + 4 * \gamma^2} * \sqrt{\frac{8 * A}{\theta - \sin\theta}} \tag{19}$$

Then, height is obtained from *(16)*.

6.3.2 Second case

On the second case, width is equal to the diameter of the circle. In that case, circle chord is smaller than track width. The formulas for r, c and θ are in *(20)* and *(21)*. This case happens when the height to width ratio is bigger than 0.5, but smaller than 0.8. This top limit was determined experimentally.

$$r = \frac{h}{2} + \frac{c^2}{8 * h} = \frac{w}{2} \tag{20}$$

$$\theta = 2 * \sin^{-1} \frac{c}{w} \tag{21}$$

Again, *(16)* is replaced in *(20)* and *(21)*, resulting in *(22)* and *(23)*.

$$c = 2 * w * \sqrt{\gamma * (1 - \gamma)} \tag{22}$$

$$\theta = 2 * \sin^{-1}\left(2 * \sqrt{\gamma * (1-\gamma)}\right) \quad (23)$$

Replacing r for $\frac{w}{2}$ in (13) and isolating w, width is calculated as shown in *(24)*.

$$w = \sqrt{\frac{8 * A}{\theta - \sin\theta}} \quad (24)$$

Height value is obtained identically as before, as *(16)*.

6.3.3 Third case

On the third case, no chord is present. It happens when the height to width ratio is over 0.8. The track area is divided in two simple geometrical shapes. The upper part is half of a circle with diameter equal to track width. Remaining part of the track is modeled as a rectangle with same width, but height equal to track height minus the radius of the circle. Area is calculated as *(25)*.

$$A = \frac{\pi * w^2}{8} + w * (h - \frac{w}{2}) \quad (25)$$

Replacing *(16)* in *(25)* and isolating w, width is obtained as *(26)*.

$$w = \sqrt{\frac{8 * A}{\pi + 8 * \gamma - 4}} \quad (26)$$

Height value is obtained identically as before *(16)*.

6.3.4 Comparison between real and predicted height and width values

After obtaining the formulas to calculate track height and width from the track predicted area and the predicted height to width ratio, those two dimensions were calculated and compared to measured values. Errors under 15% are acceptable.

Larger errors are commented below. Values obtained are on Table 6-5 and Table 6-6. Errors between predicted and real values are on the graph at Figure 6-8.

Table 6-5: Comparison between real and predicted height values

P [W]	S [mm/s]	E [J/mm]	Real Max Height [mm]	Predict Max Height [mm]	Max Height Error [%]	Real Min Height [mm]	Predict Min Height [mm]	Min Height Error [%]
572	5.83	98.1	0,5944	0,7474	25,74%	0,216	0,4661	115,79%
968	5.83	166.0	0,3474	0,3735	7,51%	0,3277	0,347	5,89%
572	0.83	686.7	1,9183	1,9701	2,70%	1,6526	1,2852	-22,23%
968	0.83	1162.1	1,5324	2,2130	44,41%	1,3897	1,6781	20,75%

Errors variate from 2.7% to 115.79%. The large errors on the less energetic track are justified by its inconstant shape, as already mentioned when predicting area in section 6.1.

Table 6-6: Comparison between real and predicted width values

P [W]	S [mm/s]	E [J/mm]	Real Max Width [mm]	Predict Max Width [mm]	Max Width Error [%]	Real Min Width [mm]	Predict Min Width [mm]	Min Width Error [%]
572	5.83	98.1	1,4826	1,3226	-10,79%	0,8958	1,2959	44,66%
968	5.83	166.0	2,3239	2,0724	-10,82%	2,0657	2,0086	-2,76%
572	0.83	686.7	2,4207	3,7979	56,89%	2,0573	1,9321	-6,09%
968	0.83	1162.1	3,1653	3,549	12,12%	2,6826	3,0145	12,37%

The track with the minimum process parameters has a large error of over 50% on its maximum predicted width. This error reflects on the minimum height error of this track as well. The predicted track should be flatter and wider. One explanation for that is this cross section's position – end of the track – combined with the high amount of added material volume and the low laser power. As the process started, the added material builds up due to the low traverse speed. The large volume of the track shields the substrate from the laser beam, reducing the energy absorbed by it and its thermal gradient. Due to this shielding effect, temperature on the substrate grows slower than expected. The lower substrate temperature does not allow a molten pool to properly

form, resulting on a thin and high track. On Figure 6-9, almost no dilution is present. It is also visible that the track is barely bond to the substrate on its beginning because of the low laser power. As the substrate gets hotter, the bond increases. By the end of the track, the bond is stablished, but some pores persist.

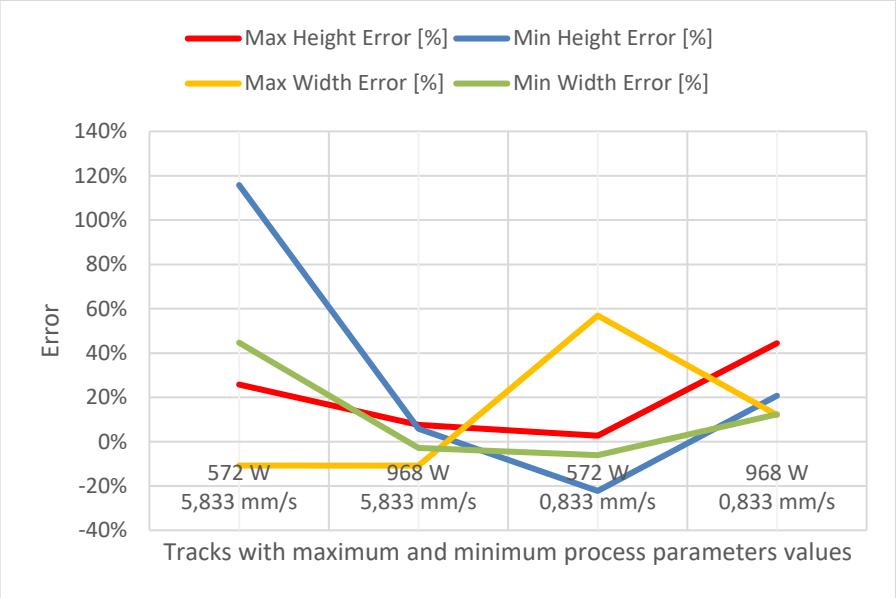

Figure 6-8: Prediction errors of track dimensions. The horizontal axis represents the different tracks cladded with the maximum and minimum process parameters values. Tracks are ordened by energy per length rate level.

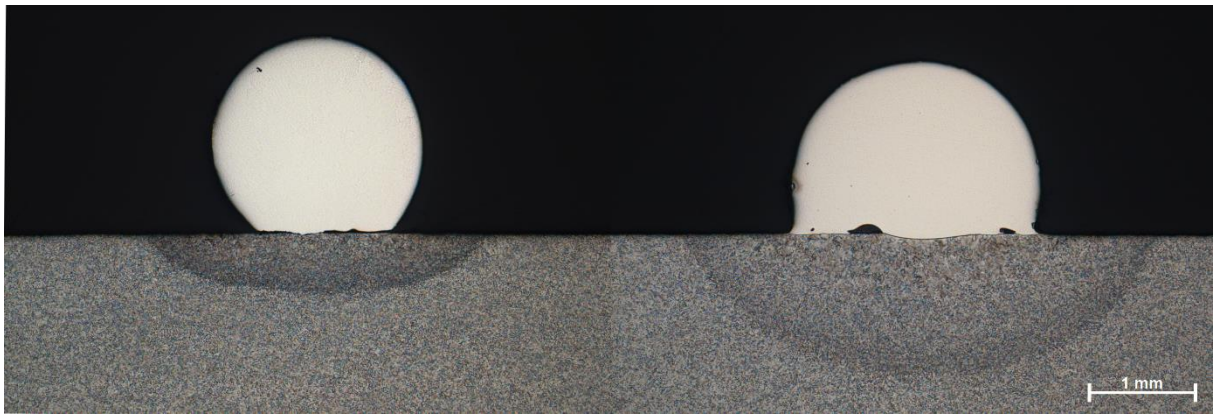

Figure 6-9: Cross sections of the beginning (left) and of the end (right) of the track with the minimum process parameters values. Molten pool width is larger on this track's end.

Height values for the most energetic track were smaller than estimated. The direct reason for that is dilution. The high laser power and slow traverse speed

generate a deep molten pool. As the material dilutes on the substrate, track becomes shorter.

For all values predicted, other errors are present. They originate from the calculated areas and height to width ratios, but also from track shape not following exactly the shapes in Figure 6-7. Intrinsic errors of the cutting procedure, cross-section positioning and measurement also contribute to the resulted errors.

The track with the most accurate predictions is the one with the highest process parameters values. The high power of the laser melts the wire, lowering its viscosity considerably, while the fast traverse speed spreads it over the substrate. Molten wire density is low enough to allow a uniform geometry along the track, as surface tensions are not high enough to create drops on it. However, dilution increases with this laser power – once it melts more of the substrate – reducing the commercial interest on this track.

Chapter 7 Conclusion and future perspectives

The results on this work improved the understanding of the scanner-based wire fed laser cladding. The main influence of traverse speed and laser power on track height, width and area were analyzed. Besides that, many other different behaviors were detected, analyzed and explained. The most important results are discussed below.

7.1 Temperature measurement

The temperature was measured on a spot 10 mm ahead of the molten pool, on the direction of cladding. Because of that, different traverse speeds affected the acquired data.

The heat spread from the molten pool to the substrate as isotherms. If those isotherms were hotter, they became slower. On faster traverse speeds, only the colder isotherms reached the measured spot while the axis were moving. When the axis stopped, however, the hotter isotherms reached this spot, leading to a temperature peak on the measurement.

As heat is conducted at relative low speeds in metals, depending on its thermal conductivity, it does not travel instantly through the substrate. A delay on the acquired data exists. This delay variates with laser power, traverse speed, room temperature, temperature of the NC machine etc. After the process, on the instant that the movement on the axis stops, the pyrometer registers an inflexion point on temperature. With this point, it was possible to predict the instant when the process began.

As temperature decreases from the molten pool to the substrate exponentially, it should be possible to calculate molten pool temperature using another pyrometer or a thermic camera. None of them would have to focus on the molten pool for that. Thus, there is no need for an equipment with a larger temperature range and protection filters against reflections, which would have been more expensive.

7.2 Main relations

Tracks with different laser powers and traverse speeds were performed to analyze the influence of those parameters on track geometry. They are resumed on Table 7-1 below.

	Laser Power ↑	Traverse Speed ↑
Height	↓	↓
Width	↑	↓
Area	-	↓
Height variation	↓	↑
Width variation	↓	↑
Area variation	↓	↑

Table 7-1: Main influences of traverse speed and laser power on track geometry and track geometry variation

If laser power is increased, the molten pool heats up, lowering its viscosity. Thus, the molten metal flows further over the substrate, leading to a flatter and wider track. The track area size stays constant.

With the increase of traverse speed, less material is added to the track, decreasing its area. As faster speeds decrease also the energy per length rate, the molten pool gets colder, leading to higher and thinner tracks.

Regarding to the geometrical variations along the tracks, the sets of parameters with the highest laser power lead to the most stable results. As a higher power laser focuses on the molten pool, more of the substrate melts. It leads to a more solid bond between track and substrate – what generates a more constant geometry – but also to a bigger dilution. Higher temperatures also increase molten pool size, generating the same effects. If dilution is too high, it compromises track wear resistance, resulting on a bad quality cladding.

7.3 Unexpected phenomena

On the track cladded with 770 W and 5.83 mm/s (Figure 5-9), there was a wire misplacement problem. Because of that, its beginning lacks on wire. The effect of that was an increased temperature. It increased its geometry variation, while generating a track that was flatter and wider than expected.

On the track cladded with 770 W and 0.83 mm/s, temperature is lower than expected. The explanation found was a shielding effect. Once this track has the highest material volume per length rate, its volume is the biggest. Its oversize was able to slightly block the substrate from the radiation of the beam. It affected temperature measurement. As this was the track of the most energetic process, it was the hottest. As soon as the axis stop, the peak on temperature measurement of this track is the hottest, confirming this fact.

On the track cladded with 572 W and 2.20 mm/s, the emitted energy was not enough to melt both wire and substrate on its beginning, generating a lack of fusion. As the temperature raised enough, all of the wire was molten at once. This extra volume generated a globular aspect on this track's beginning. This effect can be seen on Figure 5-25.

7.4 Modeling

Models for three different track geometrical features were proposed: track area, track height to width ratio, track height and width. With those models, the respective dimensions were predicted for four tracks with different sets of parameters.

The track cladded with the lowest laser power and the fastest traverse speed, however, resulted on an unstable track. It happened because the laser power was not high enough to fully bond the molten wire on the substrate at this speed. Lack of fusion and geometrical irregularities are present along the track. Those irregularities are not predicted in any of the proposed models. Thus, this track is out of the scope of the proposed models.

The first feature to be modeled was the track area. It was based on the material volume per length unit ratio from the experimental data. As only traverse speed influences the size of the track area, this dimension does not have high variations. After comparing predicted and measured values, the model successfully predicted the real dimensions of the tracks, with errors within 5%.

Later, a model for predicting the height to width ratio of the tracks was proposed. Based on experimental data, two surfaces were fitted to the measured maximum and the minimum height to width ratio values. It was observed that the individual relations between traverse speed and laser power and this ratio have the shape of power

functions. Assuming those influences as linear and independent, they were simply added together, resulting on a surface that models this ratio depending on both process parameters. Such a simple modeling aimed to analyze how good could a linear model predict the process result, but no perfect correlation was expected. Results showed that the process is far from linear. The shielding effect on lower speeds and the irregularities on the beginning of the tracks with weak laser powers affected considerably the geometry of the tracks. Those phenomena are not predicted by this linear model. Errors stayed below 10% for the slow tracks and below 20% for the faster track – only the faster track with higher laser power is considered.

The last proposed model predicted the track height and width. To do so, the shapes of the cross sections were approximated to geometrical shapes. Based on the track area and the height to width ratio, the track height and width were estimated. The obtained results presented higher errors. They originate from the errors on the measurement, area and ratio prediction, but also for the errors when approximating the track area to the geometrical shape. The model was unsuccessful in predicting those dimensions.

After testing every model, it is concluded that the track area and the height to width ratio could be efficiently predicted. Those results aid on setting the process parameters to achieve a desired geometry. Especially the height to width ratio prediction improves on the track quality for producing layers. If the track is too high and thin – with a high ratio – it is inappropriate for producing layers, increasing roughness and the amount of pores between tracks. If it is flat and wide – with a lower ratio – the overlap between tracks increases, reducing both roughness and the amount of inter-track pores.

To improve the prediction accuracy, the model should also consider the non-linear behaviors generated by the shielding effect and by the irregularity on the beginning of the tracks when cladding with too low laser power. Also, the influence of laser power on the height to width ratio changes accordingly to the actual traverse speed and vice-versa, showing interdependency between the influences of those parameters.

Bibliography

[1] KLOCKE, F. et al. Flexible scanner-based laser surface treatment. *Physics Procedia*, v. 5, p. 467–475, doi:10.1016/j.phpro.2010.08.169, 2010.

[2] KAIERLE, S. et al. Review on Laser Deposition Welding: From Micro to Macro. *Physics Procedia*, v. 39, p. 336–345, doi:10.1016/j.phpro.2012.10.046, 2012.

[3] KLOCKE, F. et al. Scanner-based Laser Cladding. *Physics Procedia*, v. 39, p. 346–353, doi:10.1016/j.phpro.2012.10.047, 2012.

[4] TOYSERKANI, E.;; CORBIN, S. e KHAJEPOUR, A. *Laser cladding*. [S.l: s.n.], 2005. p. 263

[5] ZHONG, M. e LIU, W. Laser surface cladding: the state of the art and challenges. *Proceedings of the Institution of Mechanical Engineers, Part C: Journal of Mechanical Engineering Science*, v. 224, n. 5, p. 1041–1060, doi:10.1243/09544062JMES1782, 2010.

[6] SYED, W. U. H.;; PINKERTON, A. J. e LI, L. A comparative study of wire feeding and powder feeding in direct diode laser deposition for rapid prototyping. *Applied Surface Science*, v. 247, n. 1-4, p. 268–276, doi:10.1016/j.apsusc.2005.01.138, 2005.

[7] SYED, W. U. H.;; PINKERTON, A. J. e LI, L. Combining wire and coaxial powder feeding in laser direct metal deposition for rapid prototyping. *Applied Surface Science*, v. 252, n. 13, p. 4803–4808, doi:10.1016/j.apsusc.2005.08.118, 2006.

[8] HERALIC, A. *Monitoring and Control of Robotized Laser Metal-Wire Deposition*. Chalmers University of Technology - [S.l.]. 2012.

[9] KIM, J. e PENG, Y. Plunging method for Nd : YAG laser cladding with wire feeding. v. 33, p. 299–309, 2000.

[10] LEBEDEV, V. A. Controlling penetration in mechanized welding and surfacing. *Welding International*, v. 26, n. 6, p. 459–465, doi:10.1080/09507116.2011.606162, 2012.

[11] KUMAR, A. et al. A finer modeling approach for numerically predicting single track geometry in two dimensions during Laser Rapid Manufacturing. *Optics & Laser Technology*, v. 44, n. 3, p. 555–565, doi:10.1016/j.optlastec.2011.08.026, 2012.

[12] AMINE, T.;; NEWKIRK, J. W. e LIOU, F. Case Studies in Thermal Engineering An investigation of the effect of direct metal deposition parameters on the characteristics of the deposited layers. v. 3, p. 21–34, 2014.

[13] FALLAH, V. et al. Temporal development of melt-pool morphology and clad geometry in laser powder deposition. *Computational Materials Science*, v. 50, n. 7, p. 2124–2134, doi:10.1016/j.commatsci.2011.02.018, 2011.

[14] COSTA, L. et al. A Simplified Semi-Empirical Method to Select the Processing Parameters for Laser Clad Coatings. *Materials Science Forum*, v. 414-415, n. October 2015, p. 385–394, doi:10.4028/www.scientific.net/MSF.414-415.385, 2003.

[15] OLIVEIRA, U. DE;; OCELÍK, V. e HOSSON, J. T. M. DE. Analysis of coaxial laser cladding processing conditions. *Surface and Coatings Technology*, v. 197, n. 2-3, p. 127–136, doi:10.1016/j.surfcoat.2004.06.029, 2005.

[16] PAULO DAVIM, J.;; OLIVEIRA, C. e CARDOSO, a. Predicting the geometric form of clad in laser cladding by powder using multiple regression analysis (MRA). *Materials & Design*, v. 29, n. 2, p. 554–557, doi:10.1016/j.matdes.2007.01.023, 2008.

[17] SAQIB, S.;; URBANIC, R. J. e AGGARWAL, K. Analysis of Laser Cladding Bead Morphology for Developing Additive Manufacturing Travel Paths. *Procedia CIRP*, v. 17, p. 824–829, doi:10.1016/j.procir.2014.01.098, 2014.

[18] CHEIKH, H. EL et al. Prediction and analytical description of the single laser track geometry in direct laser fabrication from process parameters and energy balance reasoning. *Journal of Materials Processing Technology*, v. 212, n. 9, p. 1832–1839, doi:10.1016/j.jmatprotec.2012.03.016, 2012.

[19] PINKERTON, A. J. e LI, L. Modelling the geometry of a moving laser melt pool and deposition track via energy and mass balances. *Journal of*

Physics D: Applied Physics, v. 37, n. 14, p. 1885–1895, doi:10.1088/0022-3727/37/14/003, 2004.

[20] NENADL, O. et al. The Prediction of Coating Geometry from Main Processing Parameters in Laser Cladding. *Physics Procedia*, v. 56, p. 220–227, doi:10.1016/j.phpro.2014.08.166, 2014.

[21] OCELÍK, V. et al. On the geometry of coating layers formed by overlap. *Surface and Coatings Technology*, v. 242, p. 54–61, doi:10.1016/j.surfcoat.2014.01.018, 2014.

[22] LEBEDEV, V. A. et al. Controlling weld geometry by means of welding equipment in mechanized and automatic consumable electrode arc welding. *Welding International*, v. 29, n. 5, p. 379–385, doi:10.1080/09507116.2014.934537, 2014.

[23] SRIMATH, N. e MURUGAN, N. Development of Mathematical Models for Prediction of Weld Bead Geometry in Cladding Mild Steel Valve Seat Rings by PTAW. *Procedia Engineering*, v. 38, p. 15–20, doi:10.1016/j.proeng.2012.06.003, 2012.

[24] SYED, W. U. H. e LI, L. Effects of wire feeding direction and location in multiple layer diode laser direct metal deposition. *Applied Surface Science*, v. 248, n. 1-4, p. 518–524, doi:10.1016/j.apsusc.2005.03.039, 2005.

[25] THOMPSON, S. M. et al. An Overview of Direct Laser Deposition for Additive Manufacturing Part I: Transport Phenomena, Modeling and Diagnostics. *Additive Manufacturing*, v. 8, p. 36–62, doi:10.1016/j.addma.2015.07.001, 2015.

[26] OCYLOK, S. et al. Correlations of Melt Pool Geometry and Process Parameters During Laser Metal Deposition by Coaxial Process Monitoring. *Physics Procedia*, v. 56, p. 228–238, doi:10.1016/j.phpro.2014.08.167, 2014.

[27] COSTA, L.;; VILAR, R. e RÉTI, T. Simulating the effects of substrate pre-heating on the final structure of steel parts built by laser powder deposition. *Solid Freeform Fabrication Proceedings*, p. 643–654, 2004.

[28] ALIMARDANI, M. et al. The effect of localized dynamic surface preheating in laser cladding of Stellite 1. *Surface and Coatings Technology*, v. 204, n. 23, p. 3911–3919, doi:10.1016/j.surfcoat.2010.05.009, 2010.

[29] FALLAH, V. et al. Impact of localized surface preheating on the microstructure and crack formation in laser direct deposition of Stellite 1 on AISI 4340 steel. *Applied Surface Science*, v. 257, n. 5, p. 1716–1723, doi:10.1016/j.apsusc.2010.09.003, 2010.

[30] JENDRZEJEWSKI, R. et al. Temperature and stress fields induced during laser cladding. *Computers & Structures*, v. 82, n. 7-8, p. 653–658, doi:10.1016/j.compstruc.2003.11.005, 2004.

[31] JENDRZEJEWSKI, R. e ŚLIWIŃSKI, G. Investigation of temperature and stress fields in laser cladded coatings. *Applied Surface Science*, v. 254, n. 4, p. 921–925, doi:10.1016/j.apsusc.2007.08.014, 2007.

[32] KIM, J. e PENG, Y. Temperature field and cooling rate of laser cladding with wire feeding. *KSME international journal*, v. 14, n. 8, p. 851–860, 2000.

[33] HOFMAN, J. T. et al. FEM modeling and experimental verification for dilution control in laser cladding. *Journal of Materials Processing Technology*, v. 211, n. 2, p. 187–196, doi:10.1016/j.jmatprotec.2010.09.007, 2011.